AFOSR-TR-95

REPORT DOCUMENTATION PAGE

0603

1. AGENCY USE ONLY (Leave blank)	2. REPORT DATE	3. REPORT TYPE AND DATES COVERED
	8/31/94	Ann. Tech. 8/1/93-7/31/94

4. TITLE AND SUBTITLE

(U) Particle Formation During the Expansion of Supercritical Solutions

5. FUNDING NUMBERS

PE - 61102F
PR - 2308
SA - BS
G - F49620-93-I-0454
(AASERT)

6. AUTHOR(S)

Pablo G. Debenedetti

7. PERFORMING ORGANIZATION NAME(S) AND ADDRESS(ES)

Princeton University
Department of Chemical Engineering
Princeton, NJ 08544-5263

8. PERFORMING ORGANIZATION REPORT NUMBER

9. SPONSORING/MONITORING AGENCY NAME(S) AND ADDRESS(ES)

AFOSR/NA
110 Duncan Avenue, Suite B115
Bolling AFB DC 20332-0001

10. SPONSORING/MONITORING AGENCY REPORT NUMBER

11. SUPPLEMENTARY NOTES

12a. DISTRIBUTION/AVAILABILITY STATEMENT

Approved for public release; distribution is unlimited

12b. DISTRIBUTION CODE

13. ABSTRACT (Maximum 200 words)

An experimental study of poly (L-lactic acid) (L-PLA) precipitation by rapid expansion of supercritical solutions in silica capillaries was carried out. The solvent was a mixture of carbon dioxide and chlorodifluoromethane. Three particle morphologies were observed: dendrites, microspheres, and irregular polyhedra (microparticles). Dendrites formed only with calibrated orifices (aspect ratio, L/D < 10). In capillaries, microspheres were always formed if the carrier fluid's density at the capillary's exit exceeded 0.0063 mol cm^{-3}; microparticles were always formed if the carrier fluid's exit density was lower than 0.0042 mol cm^{-3} (densities were calculated with a one-dimensional model of adiabatic choked flow, in conjunction with the Peng-Robinson equation of state). Microparticles formed primarily inside the silica capillary; microspheres, in the free jet after exiting the capillary. In a second study, fluorescence and transmission microscopy were used to study the distribution of pyrene (fluorescent) in L-PLA (non-fluorescent) microspheres obtained by co-precipitation from a rapidly expanding supercritical carrier. Uniform distribution of pyrene inside the polymer microspheres was achieved.

14. SUBJECT TERMS	15. NUMBER OF PAGES
Supercritical Fluids; Particle Formation; Polymer Microspheres; Materials Processing; Rapid Expansion	45
	16. PRICE CODE

17. SECURITY CLASSIFICATION OF REPORT	18. SECURITY CLASSIFICATION OF THIS PAGE	19. SECURITY CLASSIFICATION OF ABSTRACT	20. LIMITATION OF ABSTRACT
Unclassified	Unclassified	Unclassified	UL

Annual Technical Report Under
AFOSR Grant AASERT F49620-93-1-0454

Air Force Office of Scientific Research

for the Period August 1, 1993 - July 31, 1994

PARTICLE FORMATION DURING THE EXPANSION OF SUPERCRITICAL SOLUTIONS

Pablo G. Debenedetti, Professor
Principal Investigator

Department of Chemical Engineering
Princeton University
Princeton, NJ 08544-5263

1. Introduction

A fluid is said to be supercritical when its temperature and pressure are simultaneously higher than their critical point values (McHugh and Krukonis, 1986). In practice, though, the term supercritical is used to describe fluids within the relatively narrow range of temperatures and pressures ($1 < T/T_c < 1.1$; $1 < P/P_c < 2$), where subscript c denotes critical point values (Brennecke and Eckert, 1989). It is within this region that most property changes involved in the transition from a dilute gas to a dense fluid occur. Consequently, the thermophysical properties of supercritical fluids exhibit high rates of change with respect to temperature and pressure. Not all properties change at the same rate; hence the combination of thermophysical properties of supercritical fluids is quite unique. For example, supercritical fluids have liquid-like densities, kinematic viscosities that are lower than those of liquid metals, compressibilities that can be arbitrarily higher than for an ideal gas, and viscosities that are intermediate between gas- and liquid-like (Debenedetti and Reid, 1986).

Near a fluid's critical point, small changes in pressure cause very large changes in density and hence in solvent power (Kumar and Johnston, 1988). Hence, the partial decompression of a supercritical solvent (such as would occur, for example, if a supercritical fuel containing dissolved autooxidation or pyrolysis products loses ca. 200 psi in a nozzle) causes a pronounced loss of solvent power and the precipitation of dissolved solutes (Tom and Debenedetti, 1991a; Kwauk and Debenedetti, 1993). Fast expansions (e.g., 10^{-5} sec., which can be easily attained in nozzle flows) lead to appreciable supersaturations (Debenedetti, 1990). In the case of supercritical solutions, the range of attainable supersaturations is especially high because of the enormous enhancement in solvent power with respect to ideal gas conditions at the same temperature and pressure, a quantity that can be as high as 10^6. Furthermore, precipitation is triggered mechanically (by decompression) rather than thermally. Mechanical perturbations travel at the speed of sound, which favors the rapid attainment of uniform conditions within the expanding fluid. The combination of large supersaturations and small gradients is a distinguishing feature of fast supercritical expansions, and favors the formation of small and uniform particles.

In addition to the importance of understanding particle formation from the standpoint of fouling prevention in supercritical fuels, the rapid expansion of supercritical fluids (RESS) has potential application in areas as diverse as ceramics, polymer, and pharmaceuticals processing. In these and other applications, interest is driven by the

possibility of forming pure (solvent-free), small, and monodisperse particles. In our laboratory, we have used RESS to produce polymeric microparticles for use in the controlled release of therapeutic drugs (Tom and Debenedetti, 1991b; Tom et al., 1993). Despite the many uses of RESS for particle formation, there is very little quantitative understanding of the underlying physics (nucleation, growth, and coagulation at supercritical conditions), and hence it is currently very difficult to relate particle size to process conditions in realistic situations.

2. Objective

One objective of this research is to develop a realistic model of particle formation during RESS. Our existing model (Kwauk and Debenedetti, 1993) treats single-solute precipitation during one-dimensional, inviscid, partial expansions in nozzles. A more realistic model must incorporate multiple-solute precipitation, inter-particle coagulation, and friction-driven flows in constant area capillaries.

A second objective is to compare the theoretical predictions with experimental observations in our RESS apparatus. This involves measuring particle size distributions at different operating conditions, and comparing the trends with model calculations.

3. Status of the Research Effort

Single-Solute Precipitation

In single-solute precipitation, an important objective is to understand (and eventually predict) the dependence of particle size and morphology upon operating conditions. We carried out a detailed experimental study of poly (L-lactic acid) (L-PLA) precipitation during RESS, and have been able to predict the transition from microparticles to microspheres observed in experiments by means of a one-dimensional fluid mechanical model of friction-driven expansions in a capillary. L-PLA was chosen as the solute because of its use as a matrix material in devices for the controlled release of therapeutic drugs, including microspheres.This work is described in detail in the enclosed paper (Tom, Debenedetti, and Jerome, *J. Supercrit. Fluids*, 7, 9, 1994); here, we summarize the main conclusions.

The experiments were carried out in our continuous RESS unit, described in detail elsewhere (Tom and Debenedetti, 1991 a,b). An important modification was the use of silica capillaries (30 or 50 μm) of varying length as the expansion device, as opposed to the calibrated orifices used in our previous work. The solvent used was a supercritical mixture of chlorodifluoromethane ($CHClF_2$) and carbon dioxide. Relevant physical properties of the polymer and of the two co-solvents are listed in Table 1.

TABLE 1

Properties of Solute and Solvents in Single-Solute RESS Studies[a]

Compound	T_c(°C)	P_c(bar)	T_m(°C)	T_g(°C)	MW
L-PLA	---------	----------	162.5	62.0	10,000
CO_2	31	73.8	-56.5	N/A	44
$CHClF_2$	96.2	49.7	-160.1	N/A	86

[a] T_c = critical temperature; P_c = critical pressure; T_m = normal melting point; T_g = glass transition temperature; MW = molecular weight

A very large number of experiments were performed, in which the capillary's L/D ratio, as well as the pre-expansion temperature and pressure, and the composition of the supercritical stream ($CO_2/CHClF_2$ ratio) were varied. The experiments are tabulated in Tom et al. (1994). It was found that three particle morphologies occurred: dendrites, irregular polyhedra (henceforth microparticles), and microspheres. Dendrites appeared only when orifices (L/D = 9) were used. The characteristic dimension of the dendrites was greater than the orifice aperture (25 μm), indicating substantial growth in the free-jet, after the orifice.

With capillaries, two threshold densities were identified. If the density of the supercritical carrier at the exit of the capillary exceeded 0.0063 mol cm^{-3}, only microspheres were formed. If the density of the supercritical carrier at the exit of the capillary was lower than 0.0042 mol cm^{-3}, only microparticles were formed. Both morphologies were observed at intermediate exit densities. The properties of the supercritical carrier were calculated using a one-dimensional compressible flow model and

the Peng-Robinson equation of state (Peng and Robinson, 1976), with choked conditions at the capillary's exit.

The observations and calculations are easy to understand. At high exit densities, the supercritical fluid retains substantial solvent power (Tom et al., 1994); hence the bulk of the precipitation occurs in the free jet. Conversely, at lower exit densities, substantial precipitation has already occurred inside the capillary. Hence, microspheres formed largely outside the capillary; microparticles, largely inside. In general, microspheres were larger than the capillary's diameter (typically 50-100 μm), whereas the microparticles were smaller (typically < 10μm). Using the one-dimensional model, it was possible to predict (for the first time ever in RESS) the morphology of the powders, simply by calculating the carrier fluid's exit density at choked conditions for the given operating parameters (L/D ration, temperature, pressure). This is an important result. We still do not understand, however, why precipitation inside the capillaries leads to irregular particles, whereas precipitation (or at least growth) in the free jet results in spheres. More work is needed to resolve this interesting question.

Co-Precipitation of Two Solutes

An experimental study was conducted to study the co-precipitation of pyrene and L-PLA by RESS (Tom et al., 1994). Because pyrene is fluorescent and L-PLA is not, we used fluorescence and transmission microscopy to investigate the distribution of pyrene inside the L-PLA microspheres. The objective of the experiments was to investigate the influence of operating conditions upon the coating of one solute (in this case pyrene) by another (in this case L-PLA, which acted as the matrix). We were able to control the loading of pyrene in the L-PLA microspheres by changing the pyrene-to-L-PLA ratio in the mixture. Upon changing the loading of pyrene from < 0.001 wt% in CO_2 to > 0.002 wt%, the powders evolved from L-PLA microspheres with no pyrene incorporation to L-PLA microspheres uniformly loaded with pyrene. A two-column, parallel-flow configuration was used, with pyrene extracted with CO_2 in one column, and L-PLA extracted with CO_2 + $CHClF_2$ in the other one.

Our experiments are the first systematic investigation of encapsulation by RESS. The choice of solutes allowed direct observation (via fluorescence and transmission microscopy) of the distribution of pyrene inside a polymeric matrix. For this particular system (pyrene + CO_2; L-PLA + CO_2 + $CHClF_2$), the loading of the composite

microspheres was found to be sensitive to the relative amounts of the two solutes in the mixture prior to decompression. Our work demonstrates the feasibility of using RESS for producing composite particles of a polymeric matrix and embedded non-polymeric solutes. The particles are free of solvent (the solvent is a dilute gas after expansion), and they are obtained under very mild conditions. Thus, our results point to the attractiveness of RESS as a route for the production of composite microspheres for the controlled release of therapeutic drugs.

4. Current and Future Work

We are studying the co-precipitation of two solutes by RESS. Currently, we are investigating the thermodynamic aspects of the problem; specifically, we are mapping out retrograde regions (that is to say, regions of the phase diagram where the solubility of one solute increases with temperature, while that of the other solute decreases with temperature; Chimowitz et al., 1988) as a function of differences in size and energy between the two solutes. Assuming thermodynamic control (instantaneous precipitation), this calculation shows in what region one has to operate in order to achieve a desired solute ratio in the precipitate. Subsequently, we plan to incorporate nucleation kinetics, and to simulate co-precipitation (including nucleation, growth, and coagulation) in friction-driven flows under both thermodynamic and kinetic control.

Literature Cited

Brennecke, J.F., and C.A. Eckert. *AIChEJ.*, *35*, 1409 (1989).

Chimowitz, E.H., F.D. Kelley, and F.M. Munoz, *Fluid Phase Equil.*, *44*, 23 (1988).

Debenedetti, P.G. *AIChEJ.*, *36*, 1289 (1990).

Debenedetti, P.G., and R.C. Reid. *AIChEJ.*, *32*, 3024 (1986).

Kumar, S.K., and K.P. Johnston. *J. Supercrit. Fluids*, *1*, 15 (1988).

Kwauk, X., and P.G. Debenedetti, *J. Aerosol Sci.*, *24*, 445 (1993).

McHugh, M., and V.J. Krukonis, *Supercritical Fluid Extraction - Principles and Practice*, Butterworths: Boston (1986).

Peng, D.Y., and D.B. Robinson, *Ind. Eng. Chem. Fundam., 15*, 59 (1976).

Tom, J. W., and P.G. Debenedetti, *J. Aerosol Sci., 22*, 555 (1991).

Tom, J.W., and P.G. Debenedetti, *Biotech. Prog., 7*, 403 (1991b).

Tom, J.W., G.-B. Lim, P.G. Debenedetti, and R.K. Prud'homme. *ACS Symp. Ser., 514*, ch. 19 (1993).

Tom, J.W., P.G. Debenedetti, and R. Jerome. *J. Supercrit. Fluids, 7*, 9 (1994).

Published Articles

"Precipitation of Poly (L-lactic acid) and Composite Poly (L-lactic acid)-Pyrene {articles by Rapid Expansion of Supercritical Solutions". *J. Supercrit. Fluids, 7*, 9 (1994)

"Supercritical Fluids as Particle Formation Media". *NATO ASI Series E, Vol. 273*-Supercritical Fluids, Fundamentals for Application, p. 719, E. Kiran and J.M.H. Levelt-Sengers, eds. Kluwer Academic Publishers, 1994.

Presentations

"Supercritical Fluids as Particle Formation Media". NATO Advanced Study Institute on Supercritical Fluids: Fundamentals for Application, Kemer, Antalya, Turkey, July 20, 1993.

"Formation of Biologically Active Protein Powders and Polymeric Microfibers with Supercritical Anti-Solvents". 12th annual AAAR meeting, Oak Brook, Illinois, October 15, 1993.

"Rapid Expansion of Supercritical Solutions: a Comparison Between Mathematical Modeling and Experiments". AIChE annual meeting, St. Louis, November 10, 1993.

"Processing of Liquid-Crystalline Polymers Using a Supercritical Anti-Solvent: Equilibrium and Morphological Study". AIChE annual meeting, St. Louis, November 10, 1993.

"Supercritical Fluids as Particle Formation Media". Department of Chemical Engineering, Yale University, March 28, 1994.

"Supercritical Fluids as Particle Formation Media". AIChE Central Jersey Section, Princeton University, May 19, 1994.

"Supercritical Fluids as Particle Formation Media". Robert L. Mitchell Technical Center, Hoechst Celanese Corporation, Summit, New Jersey, July 14, 1994.

Personnel

Michael Winters; graduate student.

Pablo G. Debenedetti; Professor. Principal Investigator.

APPENDIX
(Reprints)

* Debenedetti, P.G., "Supercritical Fluids as Particle Formation Media", pp. 719-730 in Supercritical Fluids-Fundamentals for Application. NATO ASI Series E, Vol. 273; E. Kiran and J.M.H. Levelt Sengers, eds., Kluwer Academic Publishers, 1994

*Tom, J.W., P.G. Debenedetti,and R. Jerome, "Precipitation of Poly (L-lactic acid) and Composite Poly (L-lactic acid)-Pyrene Particles by Rapid Expansion of Supercritical Fluids", J. Supercrit. Fluids, 7, 9 (1994)

SUPERCRITICAL FLUIDS AS PARTICLE FORMATION MEDIA

PABLO G. DEBENEDETTI
Department of Chemical Engineering
Princeton University
Princeton, NJ 08544-5263
USA

ABSTRACT. There exist two routes to particle formation with supercritical fluids: rapid expansion (RESS), and the anti-solvent process (SAS). RESS is used to form fine particles of substances that are soluble in a supercritical solvent. SAS is used for sparingly soluble materials. Together, these techniques allow the processing of a wide range of materials into solid phases with useful properties and morphologies. In RESS, use is made of the sensitivity of a supercritical fluid's solvent power to small changes in pressure, to trigger precipitation mechanically. The resulting large supersaturation, coupled with the rapid attainment of uniform conditions, leads to small particles with a narrow size distribution. In SAS, the supercritical fluid is used as an anti-solvent. The solid of interest is dissolved in a liquid, and a supercritical fluid is added to precipitate the solid. Promising applications of RESS and SAS include the formation of composite drug-polymer microparticles (controlled release of drugs), of biologically active protein microparticles (controlled release of peptides and enzymes), and of molecularly oriented polymer microfibers (high performance fibers).

1. Introduction

The observation that ultrafine powders result from the decompression of supercritical fluids dates back to Hannay and Hogarth [1-3], who were the first to report the phenomenon of non-volatile solute solubility in a supercritical fluid. More than a century elapsed after Hannay and Hogarth's work before Krukonis [4] revived interest in supercritical particle formation by demonstrating its potential for processing a variety of difficult-to-comminute solids. The most important advantages of the supercritical route to solids formation are the purity of the products, the simplicity of the process(es), the possibility of producing solid phases with unique morphologies, the mildness of the operating conditions, and the wide range of materials that can be processed. The scientific understanding of RESS and SAS, and the exploration of their technical possibilities, are still in their infancy.

2. RESS

2.1. CONCEPT

Because the solvent power of a supercritical fluid is a function of its density [5,6], it can be adjusted between gas- and liquid-like extremes with moderate changes in pressure. The expansion of a supercritical solution thus leads to loss of solvent power, and hence to solute precipitation. Rapid expansions ($< 10^{-5}$ sec), such as can be easily attained in nozzles and

E. Kiran and J. M. H. Levelt Sengers (eds.), Supercritical Fluids, 719–729.

capillaries, lead to appreciable supersaturations, and hence to small particles. Pressure reduction is a mechanical perturbation that travels at the speed of sound, favoring rapid attainment of uniform conditions within the expanding fluid. The combination of large supersaturations and uniform conditions is a distinguishing feature of the RESS process, which can in principle produce small and monodisperse particles. The idea is to dissolve a solute at high pressure, exploiting the supercritical fluid's solvent power, and to precipitate it mechanically (by decompression), rather than thermally, exploiting the supercritical fluid's compressibility. The use of solvents with a moderate critical temperature (e.g., carbon dioxide: $Tc = 31^{\circ}C$) allows the processing under mild conditions of materials which would be insoluble in gases at atmospheric pressure.

2.2 FUNDAMENTALS

There are two fundamental mechanisms of phase separation: nucleation and growth [7, 8], and spinodal decomposition [9, 10]. The former is an activated process, and entails, initially, the formation of nuclei of the new phase exceeding a critical size. Such critical nuclei are in unstable equilibrium with their surroundings: subcritical nuclei disintegrate, and supercritical nuclei grow, spontaneously. When devoid of suspended impurities, metastable systems phase-separate by nucleation and growth. Spinodal decomposition is the spontaneous growth of fluctuations with arbitrary amplitude and exceeding a critical wavelength. These amplified perturbations will be density fluctuations in a pure fluid, and composition fluctuations in a mixture. Unstable systems phase-separate by spinodal decomposition. The majority of RESS applications to date involve nucleation [11], to which this discussion will be limited. Spinodal decomposition may be important in applications involving polymers [12].

The minimum (reversible) work needed to form an incompressible isotropic embryo of n solute molecules in a bulk supercritical phase at a temperature T, pressure P, and solute mole fraction y_2; and the rate per unit volume at which critical-sized embryos (nuclei) are formed, can be written as [13]

$$W_{min} = \sigma F + nkT\left[Ky_2^{eq}(S-1) - \ln S\right] \tag{1}$$

$$J = 2N_2\beta\left(\frac{\sigma v_2^2}{kT}\right)^{1/2} \bullet \exp\left\{-\frac{16\pi}{3} \bullet \left(\frac{\sigma v_2^{2/3}}{kT}\right)^3 \bullet \left[\frac{1}{\ln S - Ky_2^{eq}(S-1)}\right]^2\right\} \tag{2}$$

where σ is the interfacial tension; F, the embryo's surface area; k, Boltzmann's constant; K (T, P) (>0), the leading coefficient of the composition expansion of the solute's fugacity coefficient about its infinitely dilute limit [14]; y_2^{eq}, the solute's equilibrium mole fraction; S, the supersaturation ratio $\left(= y_2/y_2^{eq}\right)$; J, the nucleation rate; N_2, the solute's concentration in the supercritical phase; β, the solute's thermal flux (number of solute molecules crossing a unit area per unit time); and v_2, the solute's molecular volume.

Equation (2) takes into account fluid-phase non-ideality, but otherwise contains the usual assumptions and simplifications of classical nucleation theory: (i) solute molecules do not interact with each other, (ii) the embryo's radius of curvature is large with respect to molecular dimensions (capillarity approximation); (iii) an equilibrium embryo distribution is invoked in order to calculate the evaporation rate from single embryos, which is not known in general. Several alternative theories that do not rely on one or more of the above approximations have been proposed [15-17]. The critical re-examination of assumption (i), and the calculation of the thermal flux β are particularly important questions in supercritical applications. As is

commonly done in most applications involving the formation of crystalline solids, it is assumed that a single quantity, σ, can characterize what in reality are different surface energies associated with the various crystallographic orientations of a nucleus.

The calculation of particle size distributions in RESS has not been attempted until very recently [18], and much work needs to be done on this very interesting problem. Kwauk and Debenedetti [18] considered nucleation and growth during partial expansions of supercritical solutions in converging nozzles and capillaries. They developed a one-dimensional model for steady, adiabatic, sub-sonic flow. The model includes material, momentum, energy balances, and an aerosol dynamic equation. The former three are ordinary differential equations; the latter is a non-linear hyperbolic differential equation. The numerical solution to the coupled set of equations [18] yields the evolution of the particle size distribution along the axis of the expansion device. Although RESS work to date involves complete expansion to atmospheric pressure, most of which occurs in a free jet [19], partial expansions are advantageous because they maximize the amount of particle formation and growth occurring in the more controlled environment provided by the expansion device, and allow the recycling of the solvent with minimum recompression cost. Desirable post-expansion conditions would result from a compromise between high solute recovery and moderate recompression work.

Figures 1 and 2 show the effect of the extraction and pre-expansion temperatures on the calculated vapor-phase solute mole fraction, and nucleation rate profiles during nozzle expansion of a phenanthrene-carbon dioxide mixture [18]. In these calculations, the saturated mixture is in the retrograde region prior to entering the expansion device. Increasing the extraction temperature (Figure 1) leads to a smaller initial solute mole fraction, smaller supersaturations along the nozzle, precipitation closer to the nozzle's exit, shorter time for particle growth, and hence to smaller panicles. By contrast, increasing the temperature to which the mixture must be heated to prevent solvent condensation during the expansion (Figure 2) leads to higher initial supersaturations, earlier nucleation and precipitation, longer time for particle growth, and hence to larger particles. In both cases, the final particle size is determined by the fact that the mixture is in the retrograde region prior to expansion. Calculated exit conditions corresponding to Figures 1, 2 are given in Table 1, where τ is the fluid's residence time in the nozzle; dp is the peak of the particle distribution; r is the fraction of phenanthrene recovered as solid; M is the Mach number; Φ is the aerosol volume fraction; T_x is the extraction temperature, and T_{pe}, the pre-expansion temperature.

TABLE 1. Exit Conditions Corresponding to Figures 1 and 2

T	P	$10^5\tau$	dp	r	M	G	$10^4\Phi$	T_x	T_{pe}
(K)	(bar)	(sec.)	(μm)	(%)		(gh^{-1})		(K)	(K)
307.5	78.33	8.05	.037	68.8	.67	.15	8.54	330	345
305.5	75.58	8.26	.048	77.7	.68	.18	10.4	327.5	345
309.6	81.33	8.32	.027	47.9	.66	.10	5.50	332.5	345
307.5	78.33	8.05	.037	68.8	.67	.15	8.54	330	345
303.9	73.22	7.86	.044	84.1	.74	.19	9.79	330	347.5
311.0	84.07	8.65	.020	15.5	.60	.03	2.06	330	342.5
307.5	78.33	7.68	.047	86.4	.67	.19	9.81	330	348.5

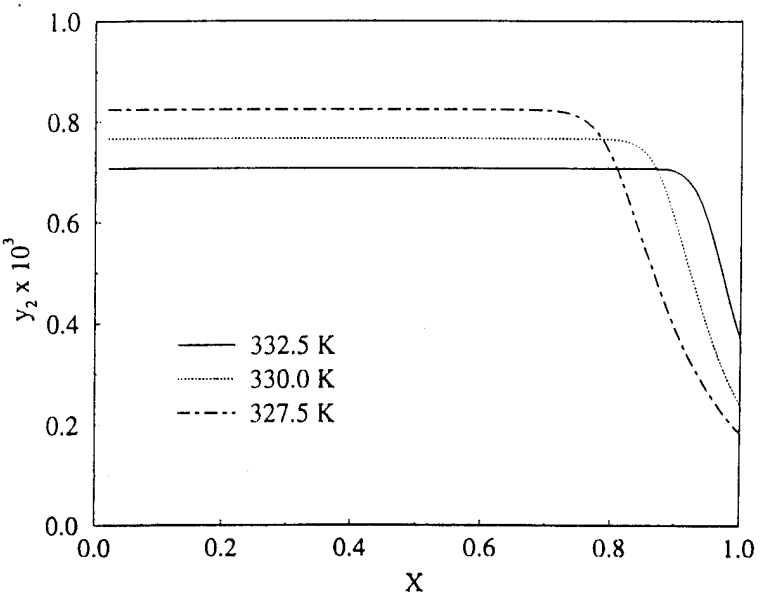

Figure 1. Phenanthrene – CO_2 RESS. Effect of extraction temperature on the fluid-phase phenanthrene mole fraction along a 30μm (inlet) x 20μm (outlet) x 10mm (length) nozzle. Extraction pressure =145 bar; pre-expansion temperature =345K; solvent flow rate =0.6 standard liters per minute.[Reproduced with permission from ref. 18. Copyright (1993, Pergamon Press Ltd.)].

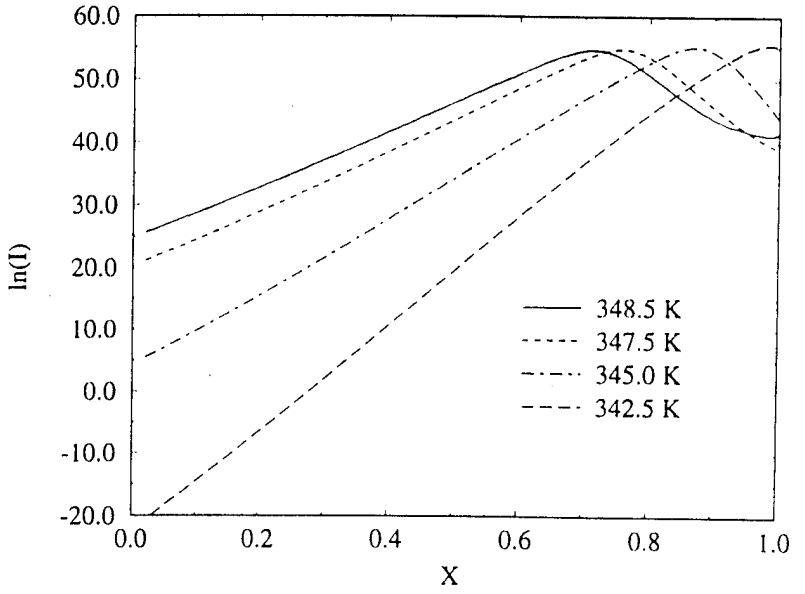

Figure 2. Phenanthrene – CO_2 RESS. Effect of pre-expansion temperature on the nucleation rate, I (m^{-3} sec^{-1}). Extraction temperature = 330K. Other conditions as in Figure 1. [Reproduced with permission from ref. 18. Copyright (1993, Pergamon Press Ltd.)].

These and many other similar calculations [18, 20] show that partial, sub-sonic expansions can lead to very small ($< 0.1\mu m$) and monodisperse particles, with high (> 90%) solids recovery. The generally much larger particle sizes, broader distributions, and extreme variability of morphology that are normally reported in the RESS literature [11] suggest that a considerable amount of inter-particle coagulation takes place in a free jet where the supercritical solution is mixed with the background gases in relatively uncontrolled fashion. The calculations shown in Figures 1 and 2 contain several simplifying assumptions. They are useful not in predicting actual numbers, but in understanding the relationship between particle size and process conditions, and in providing a rational basis for the interpretation and design of experiments. Modeling the simultaneous precipitation of multiple solutes is an interesting problem on which no work has been done; it is also (see Section 2.3) a problem of great practical significance.

2.3 APPLICATIONS

The potential applications of RESS include the comminution of labile pharmaceuticals [4, 21, 22], the formation of ceramic precursor powders [23-25], the formation of intimately mixed composite powders [24], polymer processing [20], and the formation of polymer-drug composite microparticles for the controlled release of therapeutic drugs [26, 27]. If a pharmaceutical drug is prone to degradation by heat or oxygen, the production of high-purity batches requires the use of mild and inert process conditions. Conventional methods of size reduction such as milling and grinding adversely affect the crystallinity and chemical stability of pharmaceuticals. In applications where fine powders are required, RESS with low-critical-temperature solvents allows processing at lower temperatures than conventional size-reduction methods, while at the same time providing the opportunity to form very fine, solvent-free, and monodisperse powders. In ceramic processing, RESS has been studied as a means of generating finely divided silica particles and as a novel method of producing intimate mixtures of silica and germania. During sintering, when a porous material is transformed into a dense, mechanically strong ceramic, ultrafine particles reduce the need for high temperatures and sintering aids. Since surface energy is the main driving force in sintering, smaller particles sinter faster and at lower temperatures than larger ones. In addition, small particles of ceramic components are important in applications which are subject to contamination, such as fiber and integrated optics processing. In such cases, the possibility of lowering the processing temperature using ultrafine particles made by RESS is very attractive.

The above brief summary merely illustrates some of the most interesting applications of RESS. The field has been critically reviewed recently [11]. Therefore, in this section, we discuss more recent RESS work in our laboratory aimed at forming composite drug-polymer microparticles for the controlled release of therapeutic drugs [26,27]. Controlled release is a generic name describing a wide range of systems aimed at providing temporal or spatial control of drug release in the body [28]. Of interest here are delivery systems aimed at controlling the rate at which drugs are released (temporal control). Conventional means of delivering drugs (pills, tablets) provide a single burst of drug in the blood, followed by decay in the drug concentration. It is desirable to minimize concentration variations and release the drug at a controlled rate. This provides improved therapeutic action by enhancing the drug's longevity and effectiveness in the body. One of the most common methods for the controlled release of drugs is the use of injectable polymer-drug composite microparticles. The drug is distributed uniformly in the carrier, and the polymer is degraded by body fluids over time into non-toxic products (it is bioerodible and biocompatible). Injectable microparticles are normally $< 50\mu m$. Current techniques for producing polymer-drug microspheres involve dissolution of the polymer and the drug in a common organic solvent. Microspheres are formed from this solution either by addition of an aqueous solution (with dispersing agent) which acts as an antisolvent, or by evaporation of the solvent. Another technique, spray drying, involves spraying a solution containing both the drug and the polymer into a hot gas to remove the solvent. These techniques require the removal of surfactants and organic

solvents, and can involve the use of high temperatures (spray drying). In the manufacture of microparticles intended for *in vivo* use, the removal of residual surfactants and solvents is a particularly important requirement; however, removal of these contaminants often requires prolonged vacuum or exposure to high temperatures. In contrast, RESS does not involve surfactants, organic solvents, or high temperatures, and yields a solvent-free product in a single processing step.

Figure 3 shows a composite microparticle formed by coprecipitation of lovastatin (an anti-cholesterol drug) and poly (D,L-lactic acid), a bioerodible and biocompatible polymer approved by the FDA for implants and sutures, from supercritical carbon dioxide [26, 27]. It demonstrates that it is indeed possible to microencapsulate drugs by RESS coprecipitation. At the same time, it illustrates the considerable challenges that must be overcome before the technique can be used in the production of controlled release devices. The morphology shown in Figure 3 (a single drug needle encapsulated by polymer) is not useful. Controlled release devices should consist of a uniform dispersion of finely divided particles within the polymer matrix. In order to achieve this, it is necessary to trigger heterogeneous nucleation of the polymer on the drug crystallites before the latter are allow to grow into large particles. In work in progress, we are studying this problem by varying the two solutes' supersaturation profiles along the expansion device.

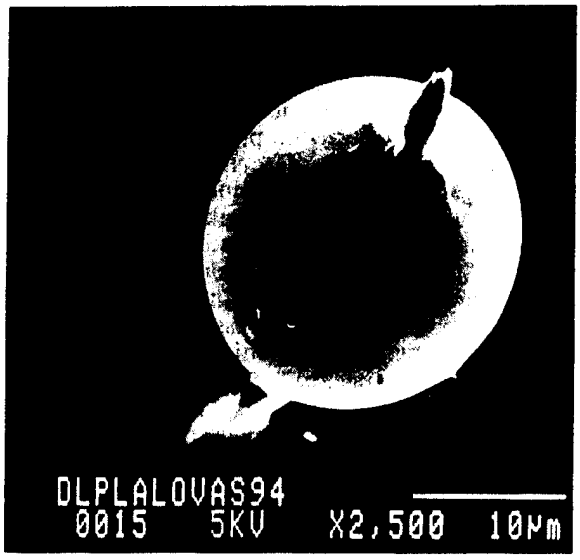

Figure 3. Scanning electron microscopy (SEM) micrograph of lovastatin needle embedded in poly (DL-lactic acid) following RESS coprecipitation from supercritical carbon dioxide. Extraction conditions: 200 bar, 55°C, pre-expansion temperature: 80°C.[Reproduced with permission from ref. 27. Copyright (1993, American Chemical Society)].

Figure 4 shows recent experiments [29] on the distribution of a low-molecular-weight compound in a polymer matrix. Shown in this figure are transmission (right) and fluorescence (left) microscopy images of poly (L-lactic) acid microparticles containing pyrene [29]. Since pyrene fluoresces, but poly (L-lactic) doesn't, and, furthermore, since pyrene doesn't form microspheres [29], the analysis implies that the polymer particles contain

uniformly dispersed pyrene. We are currently using this technique to study how the relative concentration of the polymer and the drug-analogue, low-molecular-weight compound, affect both encapsulation and distribution within the polymeric matrix.

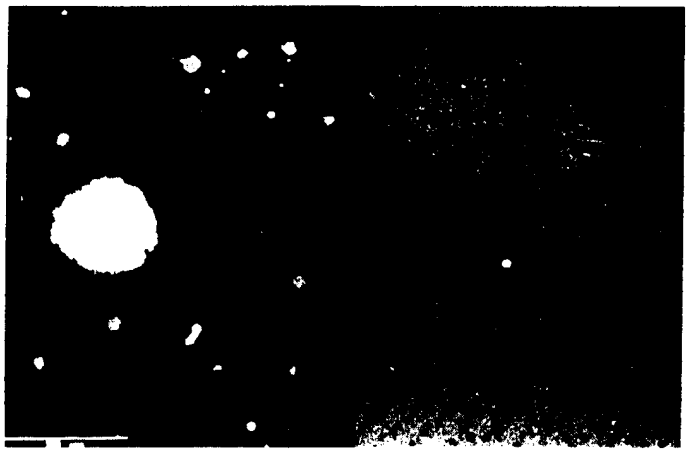

Figure 4. Fluorescence (left) and transmission (right) microscopy images of poly (L-lactic acid) microspheres containing pyrene. RESS coprecipitation form carbon dioxide - freon 22 mixture.[Reproduced with permission from ref. 29. Copyright (1993, Jean Tom)].

From these examples one can conclude that the applications of RESS have barely started to be investigated. The technique appears especially promising in biomedical applications because of the mild processing conditions, product purity, ease of processing, elimination of organic solvents and of costly separation steps, and the high added value of the products (which justifies the use of a non-traditional technology).

3. SAS

3.1 CONCEPT

In the SAS process (also referred to as gas antisolvent, GAS [30], and precipitation with a compressed fluid antisolvent, PCA [31]) the solid of interest is dissolved in a liquid, and a supercritical fluid having low solvent power with respect to the solute, but miscible with the liquid, is added to precipitate the solid. When this process is operated in batch mode [30,32], the supercritical fluid is dissolved in an excess of liquid phase. This can cause appreciable volumetric expansion, and the resulting decrease in the liquid's cohesive energy density causes the solute to precipitate. Recent studies have addressed the equilibrium thermodynamics of solid solubility in expanded liquids [31,33].

When the process is operated in continuous mode [31, 34, 35], the liquid and supercritical phases are fed continuously into a precipitator. Very small, sub-millimeter droplets are created by flowing the liquid solution through a nozzle. The pressure drop across this nozzle

is not large, as in the RESS process; here, the pressure drop is used merely to form the small droplets. The droplets are contacted with an excess of supercritical fluid. Two processes then occur: dissolution of the supercritical fluid in the liquid droplet, and, under suitable operating conditions, evaporation of the liquid into the supercritical fluid. This causes the precipitation of dry powders. Figure 5 [35] shows the experimentally measured phase boundaries of the ternary system composed of dimethyl sulfoxide (DMSO; solvent) + carbon dioxide (antisolvent) + a para-linked aromatic polyamide (solute). The three regions denote two-phase vapor-liquid equilibrium [VL; carbon dioxide-rich (V) + DMSO-rich liquid (L) with dissolved polymer]; three-phase vapor-liquid-solid equilibrium [VLS; carbon dioxide-rich (V) + DMSO-rich liquid (L) + solid polymer (S)]; and two-phase solid-fluid equilibrium (supercritical carbon dioxide-rich (F) + solid polymer (S)]. Operation in the FS region leads to polymer precipitation and removal of the solvent.

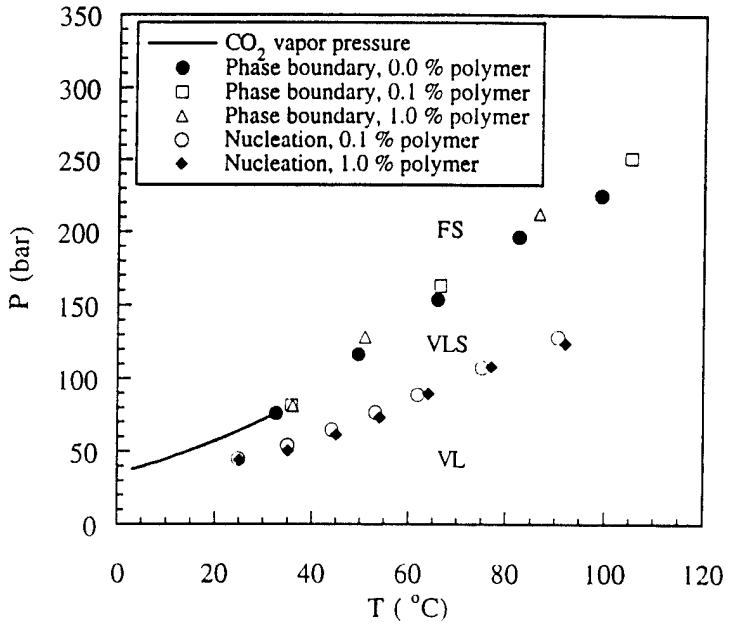

Figure 5. Equilibrium phase boundaries for CO_2+DMSO+polyamide 8 system, for 12.2% (w/w) DMSO, on a polymer-free basis. Polymer concentration in DMSO solutions: 0,0.1, and 1% (w/w). [Reproduced with permission from ref. 35. Copyright (1993, American Chemical Society)].

To date, modeling of the SAS process has been limited to phase equilibrium calculations [31,33]. The relationship between particle size, morphology, and process conditions, has not been investigated theoretically. This is fascinating but formidable problem involving drop and jet formation and breakup, mass transfer to and from the droplets, solvent evaporation, nucleation, and growth.

3.2 APPLICATIONS

SAS has been used to recrystallize difficult-to-comminute explosives [30], to form biologically active microparticulate protein powders [34], and to process polymers into interesting and useful morphologies [31,35].

Controlled release systems for peptides and proteins offer several advantages over conventional solution formulations [34]. These include decreased injection frequency,

minimization of peak and trough drug levels, increased patient compliance for chronic indications, and the potential for reducing the total administered drug dose. Most controlled release systems currently under investigation for peptides and proteins are injectable microparticulate systems consisting of peptide or protein particles dispersed within a bioerodible polymer matrix. Drug particles in the 1- to $5\mu m$ size range are ideally required for incorporation into injectable microspheres. Severe problems exist in the application of conventional size reduction techniques to the production of peptide and protein panicles in this size range. These include denaturation, small yields, broad size distributions and the need for additional processing steps in the case of wet processes. There is therefore considerable incentive for the exploration of alternative methodologies that will lead to biologically active peptide and protein particles in the $< 5\mu m$ size range. Figure 6 shows the particle distribution obtained from SAS-processing of insulin using DMSO as solvent, and carbon dioxide as anti-solvent. Similar results were obtained with N,N-dimethylformamide (DMFA) as solvent [34]. *In-vivo* tests on laboratory rats [34] showed that the insulin powders retained all of their biological activity. These results, together with those of an earlier study [27] suggest that SAS offers considerable advantages over traditional methods for the production of biologically active fine powders of proteins, peptides, and enzymes.

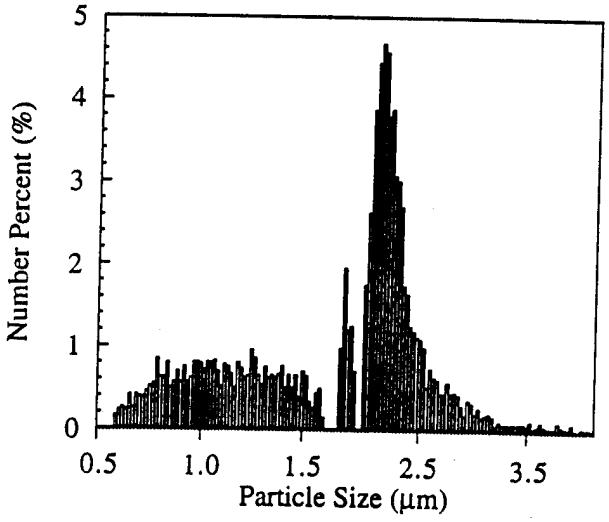

Figure 6. Particle size distribution for SAS-processed insulin. T= 35°C; P = 86.2 bar; 15 mg insulin/ml DMSO; anti-solvent CO_2. [Reproduced with permission from ref. 34. Copyright (1993, John Wiley and Sons, Inc.)].

Figure 7 shows a bundle of microfibers of a para-linked aromatic polyamide obtained by SAS processing using DMSO as solvent and carbon dioxide as the supercritical anti-solvent [35]. Individual microfibers are approximately $0.1\mu m$ thick. This material is a thermally stable polymer that can be used to produce high-modulus and heat-resistant fibers. In these experiments, the liquid droplets coalesce into a thin film which is drawn by the faster-flowing supercritical continuum. Thus, the morphology is not inconsistent with shear-induced chain reorientation during nucleation.

These two examples illustrate some of the interesting and useful morphologies that can be produced by the SAS process. This technique is more recent than RESS, and has received correspondingly less attention. In particular, no attempt has yet been made to relate process

conditions to particle size and morphology quantitatively, although interesting and plausible qualitative interpretations have been proposed [31].

Many materials of interest, such as biomolecules and polymers, have very limited solubility in the usual supercritical fluids. Thus, the SAS technique is of great interest, because it allows the processing of many such materials under mild conditions, into useful, often unique morphologies, and, with a suitable choice of operating conditions, yields dry, pure, solvent-free products.

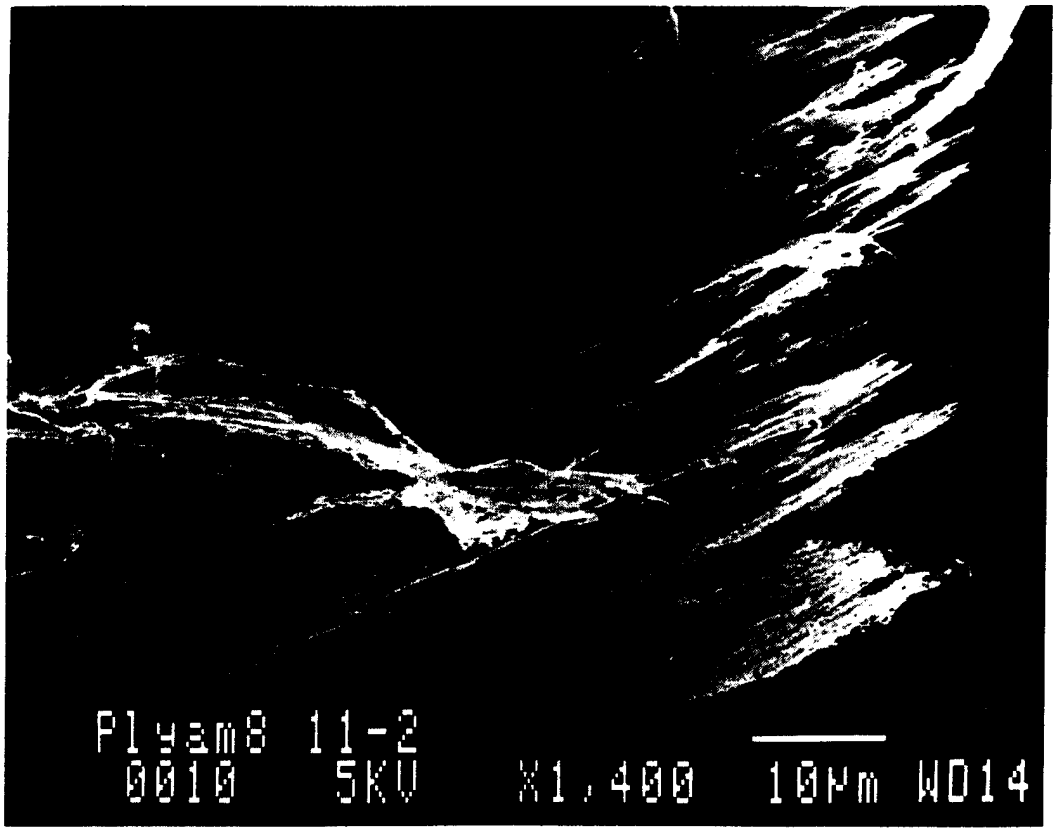

Figure 7. Fiber bundle of SAS-processed polyamide 8. T= 40°C; P = 103.4 bar; 0.03% (w/w) polyamide in DMSO; anti-solvent CO_2. [Reproduced with permission from ref. 35. Copyright (1993, American Chemcial Society)].

Acknowledgment

It is a pleasure to thank the National Science Foundation (Grant CTS-9000614), the Air Force Office of Scientific Research (Grant F49620-93-1-0454), the John Simon Guggenheim Memorial Foundation, the Camille and Henry Dreyfus Foundation, and Enzytech, Inc., for supporting this work. I am very grateful to my collaborators Xianmin Kwauk, Dr. Jean Tom, and Dr. Sang-Do Yeo: this work would not have been possible without their knowledge, skill and insight.

REFERENCES

[1] Hannay, J.B.; Hogarth, J. *Proc. Roy. Soc. London* **1879,** 29, 324.
[2] Hannay, J.B.; Hogarth, J. *Proc. Roy. Soc. London* **1880,** 30, 178.
[3] Hannay, J.B.; Hogarth, J. *Proc. Roy. Soc. London* **1879,** 30, 484.
[4] Krukonis, V.J. *Supercritical Fluid Nucleation of Difficult-to-Comminute Solids* **1984,** AIChE Fall Meeting, San Francisco, CA, paper 140f.
[5] Kumar, S.K.; Johnston, K.P. *J. Supercrit. Fluids* **1988,** 1, 15.
[6] Harvey, A.H. *J. Phys. Chem.* **1990,** 94, 8403.
[7] Becker, R; Döring, W. *Ann. Phys. (Leipzig)* **1935,** 24, 719.
[8] Abraham, F.F. *Homogeneous Nucleation Theory. The Pretransition Theory of Vapor Condensation;* Academic Press: New York, 1974.
[9] Cahn, J.W. *Acta Metall.* **1961,** 9, 975.
[10] Langer, J.S. *Acta Metall.* **1973,** 21, 1649.
[11] Tom, J.W.; Debenedetti, P.G. *J. Aerosol Sci.* **1991,** 22, 555.
[12] Lele, A.;Shine, A.D. *AIChEJ* **1992,** 38,742.
[13] Debenedetti, P.G. *AIChEJ* **1990,** 36, 1289.
[14] Debenedetti, P.G.; Kumar, S.K. *AIChEJ* **1986,** 32, 1253.
[15] Ellerby, H.M.; Reiss, H. *J. Chem. Phys.* **1992,** 97, 5766.
[16] Nowakowski, B.; Ruckenstein, E *J. Chem. Phys.* **1991,** 94, 1397.
[17] Zeng, X.C.; Oxtoby, D.W. *J. Chem. Phys.* **1991,** 94, 4472.
[18] Kwauk, X.; Debenedetti, P.G. *J. Aerosol Sci.* **1993,** 24, 445.
[19] Matson, D.W.; Fulton, J.R.; Petersen, R.C.; Smith, R.D. *Ind. Eng. Chem. Res.* **1987,** 26, 2298.
[20] Kwauk, X.; Debenedetti, P.G. Unpublished work. **1993**
[21] Larson, K.A.; King, M.L. *Biotech. Prog.* **1986,** 2, 73.
[22] Chang, C.J.; Randolph, A.D. *AIChEJ* **1989,** 35, 1876.
[23] Matson, D.W.; Petersen, R.C.; Smith, R.D. *Adv. Cermn. Mat.* **1986,** 1, 242.
[24] Matson, D.W.; Petersen, R.C.; Smith, R.D. *Adv. Ceram.* **1987,** 21, 109.
[25] Adschiri, T.; Kanazawa, K.; Arai, K. *J. Am. Ceram. Soc.* **1992,** 75,1019.
[26] Debenedetti, P.G.; Tom, J.W., Yeo, S.-D.; Lim, G.-B. *J. Contr. Rel.* **1993,** 24, 27.
[27] Tom, J.W.; Lim G.-B.; Debenedetti, P.G.; Prud'homme, R.K. In *Supercritical Fluid Engineering Science-Fundamentals and Applications* F. Kiran; J.F. Brennecke Eds.; ACS Symp. Ser. 514, American Chemical Society Washington, DC, 1993, Chapter 11.
[28] Langer, R.S. *Science* **1990,** 249,1527.
[29] Tom, J.W. *Supercritical Solutions: Particle Formation Experiments and Integral Equation Calculations* **1993,** Ph.D. Thesis, Princeton University.
[30] Gallagher, P.M.; Coffey, M. P.; Krukonis, V.J.; Hillstrom, W.W. *J. Supercrit. Fluids* **1992,** 5, 130.
[31] Dixon, D.J.; Johnston, K.P.; Bodmeier, R.A. *AIChEJ* **1993,** 39,127.
[32] Chang, C. J.;Randolph, A.D. *AIChEJ* **1990,** 36, 939.
[33] Dixon, D.J.; Johnston, K.P. *AIChEJ* **1991,** 37, 1441.
[34] Yeo, S.-D., Lim, G.-B.; Debenedetti, P.G.; Bernstein, H. *Biotech. Bioeng* **1993,** 41, 341.
[35] Yeo, S.-D.; Debenedetti, P.G.; Radosz, M.; Schmidt, H.-W. *Macromolecules,* **1993,** 26, 6207.

Precipitation of Poly(L-lactic acid) and Composite Poly(L-lactic acid)–Pyrene Particles by Rapid Expansion of Supercritical Solutions

Jean W. Tom[†] and Pablo G. Debenedetti*

Department of Chemical Engineering, Princeton University, Princeton, NJ 08544

Robert Jerome

Center for Education and Research on Macromolecules (CERM), University of Liège, Sart-Tilman, B6 4000 Liège, Belgium

Received September 29, 1993; accepted in revised form January 6, 1994

The rapid expansion of supercritical solutions (RESS) was explored as a novel route to the formation of microparticles and microspheres useful in controlled drug-delivery applications. Poly(L-lactic acid) was dissolved in supercritical CO_2 with $CHClF_2$ as a cosolvent and precipitated by RESS. The polymer's solubility and its molecular weight in solution were found to depend on processing time because of sample polydispersity. The morphology of the precipitate (microparticles, microspheres, agglomerates, or dendrites) was examined as a function of the type of the expansion device (orifices or capillaries), preexpansion temperature, and solvent composition. Dendrites were the most common morphology when using orifices. Microsphere formation using capillaries occurred with low preexpansion temperatures and low length-to-diameter ratios. A one-dimensional fluid mechanical model of the solvent's expansion in a capillary indicates that microspheres were formed preferentially when the fluid's exit density was high, suggesting that substantial precipitation occurred outside the capillary. In the first comprehensive study of the effects of process conditions on the composite powders formed by RESS coprecipitation, pyrene (a nonpolymeric fluorescent solute) was coprecipitated with poly(L-lactic acid) from supercritical CO_2–$CHClF_2$ solutions. Fluorescence and transmission microscopy allowed the observation of pyrene in the coprecipitate. These experiments showed clearly the uniform incorporation of pyrene microparticles within polymer microspheres, and thus, the feasibility of RESS as a technique for the coprecipitation of composite particles with multiple substances.

Keywords: poly(hydroxy acids), supercritical carbon dioxide, rapid expansion, particle formation, coprecipitation, modeling

INTRODUCTION

The rapid expansion of supercritical solutions (RESS)[1] is a promising new technique for the production of small and uniform particles. It can lead to solvent-free, drug-loaded polymer microspheres for controlled drug-release of therapeutic agents[2,3] ultrafine ceramic precursor powders (both chemically pure and intimate mixture(s) thereof);[1,4–9] ceramic films,[10] polymeric powders and fibers,[1,11,12] and ultrafine crystalline powders of pharmaceutical or organic compounds.[13–16]

In RESS, a nonvolatile solute is dissolved in a supercritical fluid. The resulting solution is highly compressible in the vicinity of the solvent's critical point. Due to its high compressibility, the density and hence, solvent power[17,18] of a supercritical fluid can be adjusted between gas- and liquid-like extremes with moderate changes in pressure. The expansion of supercritical solutions leads to loss of solvent power, and hence, to solute precipitation. The ratio of actual solubility to the solu-

† Current Address: Merck Research Laboratories, P.O. Box 2000, Rahway, NJ 07065

0896-8446/94/0701-0009$5.00/0

bility predicted by assuming ideal gas behavior at the same pressure and temperature (enhancement factor) can be as high as 10^6 for dilute mixtures of nonvolatile solutes in supercritical solvents.[19] Because of the high enhancement factors, the expansion of supercritical solutions can result in large supersaturations. Furthermore, pressure reduction is a mechanical perturbation that travels at the speed of sound, favoring rapid attainment of uniform conditions within the expanding fluid. The combination of high supersaturation ratios and a rapidly propagating mechanical perturbation is a distinguishing feature of the RESS process. The former leads to small particles; the latter to a narrow particle size distribution. The key idea is then to dissolve a solute at high pressure, exploiting the supercritical fluid's solvent power, and to precipitate it mechanically (by rapid expansion), exploiting the solvent's high compressibility, leading, in principle, to the formation of small and monodisperse solute particles. The use of solvents with a moderate critical temperature (e.g., CO_2: $T_c = 31$ °C) allows the processing under mild conditions of a wide variety of materials that are insoluble in gases at atmospheric pressure.

The ultimate goal of the present research is to fabricate polymeric microspheres or microparticles loaded with pharmaceuticals for controlled drug-delivery applications using the technique of rapid expansion of supercritical solutions. Controlled drug delivery is a generic term describing a wide range of systems aimed at providing temporal or spatial control of the release of therapeutic drugs in the body (for recent reviews, see Langer,[20] Rosen et al.,[21] Langer and Wise,[22] and Langer and Peppas[23]). Of interest here is controlling the rate at which the drugs are released. Controlled drug-release can minimize both the variations in the drug's concentration in the body and the quantity and frequency of drug dosages, thereby improving therapeutic action by enhancing the drug's effectiveness. One method of administering controlled drug formulations is through injection of polymer–drug microspheres and microparticles (<100 μm). In these formulations, the drug is typically distributed uniformly in a polymer carrier. In most applications, the polymer is degraded by body fluids over time (i.e., it is biodegradable or bioerodible) to non-toxic products (i.e., it is biocompatible). One such polymer is poly(L-lactic acid) which degrades to L-lactic acid, and has been approved by the Food and Drug Administration for in vivo use as sutures, bone repair implants, and some controlled drug-delivery formulations.[24] In such formulations, the drug is released through a combination of diffusion through the polymer matrix, and surface erosion of the polymer. Current techniques for producing polymer–drug matrices involve dissolution of the polymer and drug in a common organic solvent.[25] Microspheres are formed by removal of the organic solvent, addition of an aqueous solution (with dispersing agents) which acts as an anti-solvent, or spray-drying the solution into a hot gas to remove the solvent. Microparticles can be formed by melt-pressing the polymer and drug, and subsequent grinding. The disadvantages of these conventional methods are the use of organic solvents and surfactants which must be removed before in vivo use, and high temperatures which may affect the stability of the pharmaceutical compound. In contrast, RESS does not involve surfactants, liquid organic solvents, or high temperatures (if a low-critical-temperature solvent is used), and it yields a solvent-free product in a single processing step.

To date, most work with RESS has been aimed at exploring its applications to a wide range of materials (for a recent review, see Tom and Debenedetti[26]). Recent studies have begun to focus less on the novelty of RESS and more on a systematic investigation of the effects of process variables upon product characteristics.[11,15] To understand the relationship between process conditions and particle size, a theoretical framework for RESS is gradually being developed.[11,27,28]

Commercially available L-PLA and other poly(hydroxy acids) ($\overline{M}_w \approx 5000$–$6000$, $\overline{M}_w/\overline{M}_n \approx 2$) have been processed by RESS and found to be soluble in supercritical CO_2 and supercritical CO_2 with acetone as a cosolvent.[2] In these continuous experiments, the polydispersity of the polymer affected the evolution of processing over time. The supercritical solvent preferentially extracted polymer material of lower molecular weight, thereby affecting the molecular weight, polydispersity, and solubility of the polymer during the course of an experiment. After sufficient preconditioning in pure CO_2, the molecular weight of the extracted L-PLA was typically 2000–3000, and the solubility in CO_2 was typically <0.1 wt %. L-PLA microspheres and microparticles were formed by RESS processing, and the resulting precipitate was found to have a degradation profile similar to the commercial starting material.[2] Coprecipitation by RESS of poly(DL-lactic acid) (DL-PLA) and lovastatin, a anticholesterol pharmaceutical drug, resulted in a range of precipitate morphologies including polymer-coated drug needles.[3] The main finding of these previous studies is that RESS is a feasible and potentially attractive method to process poly(hydroxy acids) and pharmaceutical compounds into devices useful for controlled drug-delivery.

In this work, we systematically measure the effects of key process variables on RESS of non-commercial, monodisperse L-PLA of higher molecular weight ($\overline{M}_w$ = 10000), and we interpret some of these effects using a simple model of the solvent-expansion process during RESS. Finally, the distribution of pyrene, a model fluorescent solute, in L-PLA particles formed during RESS coprecipitation of pyrene and L-PLA is examined using fluorescence microscopy. This work is the first systematic study of the effects of process conditions on coprecipitation by RESS.

In this paper, we first present the materials and methods used in the experiments. This is followed by discussions of solubility measurements in $CO_2/CHClF_2$

TABLE I
Properties of Materials Used in This Study

Compound	Formula	T_c (°C)	P_c (bar)	T_m (°C)	T_g (°C)	MW
L-PLA	H[-OC*H(CH_3)C(O)-]$_n$OH	—	—	162.5	62.0	≈10,000
pyrene	$C_{16}H_{10}$	—	—	156	N/A	202.24
carbon dioxide	CO_2	31.0	73.8	−56.5	N/A	44.01
chlorodifluormethane	$CHClF_2$	96.2	49.7	−160.1	N/A	86.47

* Represents chiral center

mixtures in a continuous apparatus and of RESS-processing of L-PLA. An analysis of experimental trends using a simple one-dimensional solvent expansion model and an experimental study of RESS coprecipitation of L-PLA and pyrene complete the paper.

MATERIALS

The L-PLA used in this study ($\overline{M}_w$ = 10000, polydispersity ($\overline{M}_w/\overline{M}_n$) = 1.15) is synthesized using aluminum isopropoxide as an initiator for the ring-opening polymerization of L-lactides. L-lactide is purchased from Boehringer and recrystallized three times from dried ethyl acetate at 60 °C. The monomer is dried for 24 h at 25 °C under reduced pressure (10^{-2} mm Hg) before polymerization. Aluminum isopropoxide (Fluka) is distilled under vacuum (10^{-2} mm Hg) and dissolved in dry toluene. In a nitrogen-purged glass reactor, monomer, solvent, and initiator are added, and the reaction is stopped by adding an excess (relative to the initiator) of 2N HCl solution. The initiator residues are extracted four times with a dilute acid solution. The reaction mixture is then washed with water to a neutral pH and the polymer is precipitated into an excess of methanol, filtered, and dried under vacuum to a constant weight. This technique has been described in detail.[29,30] L-PLA with this specific polydispersity cannot be obtained commercially because commercial synthetic techniques (polycondensation, or ring-opening polymerization of lactides with stannous octoate) typically produce material with a polydispersity greater than two. It is expected that with a polymer of lower polydispersity, the polymer's molecular weight and solubility will be constant over the course of the experiments, after sufficient preconditioning to remove the oligomers.

Commercially available pyrene ($C_{16}H_{10}$) (Aldrich Chemical Co., 98%), a fluorescent, aromatic compound, is used as a model non-polymeric solute in coprecipitation experiments with L-PLA. The fluorescence of pyrene allows the use of fluorescence microscopy to examine its distribution in the powders produced by coprecipitation with a non-fluorescent polymer. The solubility of pyrene in supercritical CO_2 has already been studied; the highest measured solubility is 0.3 wt % at 55 °C and 245 bar.[31,32]

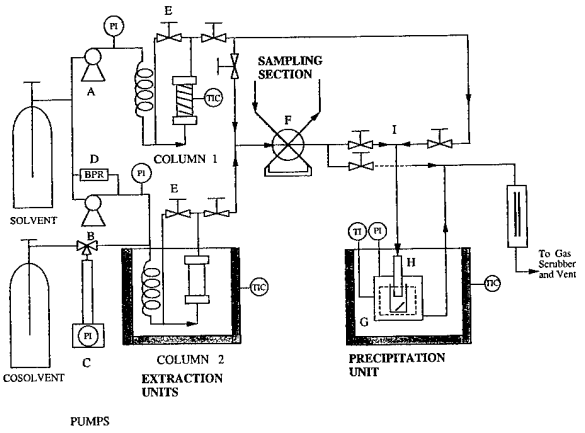

Figure 1. Schematic of RESS apparatus.

Mixtures of carbon dioxide (Bone Dry Grade >99.8% MG Industries or Airco) and chlorodifluoromethane (>98%, Atochem) are used as the supercritical fluid in the solubility measurements and RESS experiments. Chlorodifluoromethane has been shown[11] to be a better solvent than CO_2 for polymers such as poly(acrylics) and poly(hydroxy acids). The use of a better solvent leads to less fractionation of the polymer because of the greater capacity for dissolving material of higher molecular weights. Table I lists some physical properties of the materials used in this study.

EXPERIMENTAL APPARATUS AND METHODS

The experimental apparatus for RESS is shown schematically in Figure 1. Modifications to the apparatus not detailed in previous descriptions[2,3,15,26] include the addition of a syringe pump (pump C) to meter $CHClF_2$ (the cosolvent), and a second column (column 2) packed with the non-polymeric solute. Here, we give a general description of the equipment's operation and a more detailed description of the new modifications. The apparatus

can be divided into three units: extraction, sampling, and precipitation.

In the extraction unit, the two columns (stainless steel, 12" length, 1" O.D.) operate in parallel, with column 1 containing L-PLA (typically 4–5 g) and column 2 containing pyrene (9–10 g). CO_2 is delivered to both columns with a reciprocating plunger, positive displacement pump (LDC duplex minipump®) with two independent heads, [A] for column 1 and [B] for column 2. $CHClF_2$ is metered into column 1 by a syringe pump [C] (ISCO, Model 500D). The pressure in column 1 is set by a back-pressure regulator [D] (Tescom, model 26-1722-24-043) which controls the flow rate of CO_2 into column 1. In the extraction unit, the solvent or solvent mixture is pumped to desired pressure and preheated to extraction temperature, and then extracts the solute of interest. Bypass valves [E] at the columns' exit are used to dilute (if necessary) the saturated supercritical solution exiting the column. In coprecipitation experiments, the two supercritical solutions (L-PLA in $CO_2/CHClF_2$ and pyrene in CO_2) do not mix until they reach the precipitation unit.

The solution then enters the sampling section via a six-port injection valve [F] (Valco PN C6W). When both columns are in operation during coprecipitation, the pyrene–CO_2 solution will bypass the sampling section. Measurements of solubility are done separately from the RESS experiments, with either column 1 or column 2 in operation. The solution exiting from the column enters a sample loop (10 mL) before flowing into the precipitator. During collection of samples, the CO_2 or $CO_2/CHClF_2$ in the loop is evaporated, and approximately 50–60 mL of chloroform are used to flush the solute from the sample loop. The sample is concentrated to dryness and rediluted with the appropriate solvent to 0.5 to 2 mL for analysis by either gel-permeation chromatography (GPC) or high performance liquid chromatography (HPLC). The polymer samples are analyzed by GPC (polystyrene–divinyl benzene column, Polymer Laboratories PLgel 5 μm, 500 Å, 30-cm length); mobile-phase: chloroform at 1 mL min^{-1}; refractive index detector (Knauer, Type 198). The pyrene samples are analyzed by HPLC (C18 column Phenomenex, Bondclone 10, 3.9 mm × 30 cm); mobile-phase: methanol at 1 mL min^{-1}; UV detector at 240 nm; Hewlett Packard 1050 Chromatography System.

The solution leaves the sampling section and flows to the crystallizer [G] (Ruska 2329-800) where it flows through an expansion device of diameter 25–50 μm. A cable heater [H] (Watlow 62H65A3X) wrapped around the tube leading to the expansion device is used to heat the solution to a desired preexpansion temperature. Adequate preexpansion temperatures are needed to prevent phase changes in the solvent upon expansion (condensation) and plugging of the expansion unit due to premature precipitation. In coprecipitation, the two solutions are mixed at the point where cable heating begins [I]. Check valves (Autoclave Engineers) direct the flow of the fluid after the columns to prevent mixing of the two column streams prior to point [I].

The expansion devices used in this work are more accurately described as orifices or capillaries. The orifices consist of a 4.76-mm diameter by 0.25-mm thick stainless steel disk with a 25-μm laser-drilled hole (Advanced Laser Systems, Waltham, Ma.). The orifice is held in place by a stainless steel screw-cap. The capillaries are silica tubing (Polymicro Technologies, Phoenix, AZ) with inner diameters of 30 or 50 μm. The tubing is cut to desired length (0.5 to 2.0 mm) and is held in place using a ferrule and nut. In the case of the orifice, the length to diameter ratio (*L/D*)) is fixed at 9.4, while the *L/D* ratio of the capillaries can be varied from 100 to 500.

When the supercritical solution flows through the expansion device, it experiences a rapid decompression which results in precipitation of the solutes. The solutes are deposited on a microscope slide in a glass beaker placed inside the crystallizer. The supercritical solvent, now a gas, is passed through a rotameter and vented. Typical flow rates are 0.5–1 standard liters per minute (SLPM). The pressures and temperatures throughout the extraction, sampling and precipitation units are monitored with pressure gauges (Heise Models 910A and 910B) and thermocouples (Omega Type J).

A number of analytical tests are performed on the precipitated powders. Detailed observation of particle morphology is obtained by scanning electron microscopy (SEM) (JEOL JSM-840; samples coated with gold–palladium). Fluorescence microscopy with a confocal imaging system (BioRad MRC 600) linked with a microscope equipped for epifluorescence (Nikon Optiphot-2) is used to observe the distribution of pyrene in the coprecipitate. Nuclear magnetic resonance spectroscopy (GE QE-300) in deuterated chloroform ($CDCl_3$) is used to quantify the composition of coprecipitated powder. Property characterization tests such as differential scanning calorimetry (DSC) (Perkin–Elmer System 4), powder x-ray diffraction (using either Philips XRG-3000 generator with a Philips–Norelco diffractometer, or Scintag Inc., PAD-5), BET nitrogen gas adsorption (Quantachrome model QS-7), and chromatography (described earlier) are done on both the starting and precipitated material. In addition to solubility information, molecular weight and polydispersity are calculated from GPC. Polymer-degradation experiments are done both on the starting and on the precipitated L-PLA to determine the effect of RESS processing on the rate at which the material hydrolyses to L-lactic acid. In these experiments, the polymer (10–40 mg) is suspended in 100–125 mL of aqueous phosphate buffer solution (pH = 7.4). The buffer is placed in a 37 °C shake bath for up to 4000 h. The concentration of L-lactic acid is monitored by reacting an aliquot of the buffer solution with nicotinamide adenine dinucleotide (NAD) and lactate dehydrogenase (Sigma diagnostic kit 826-B). The aliquot's UV ab-

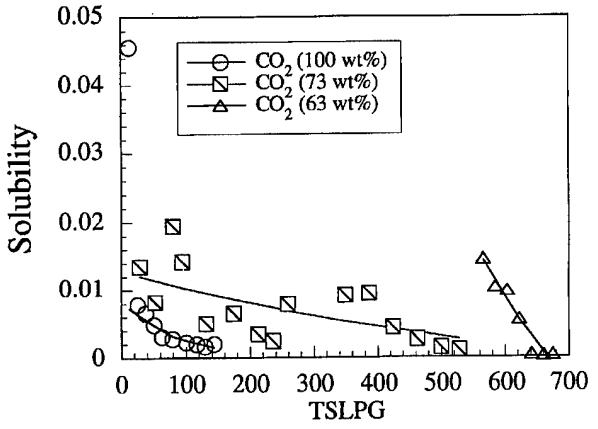

Figure 2. Solubility of L-PLA as a function of TSLPG (total standard liters solvent per gram polymer) using extraction conditions of 55 °C and 200 bar. Line is best fit through data.

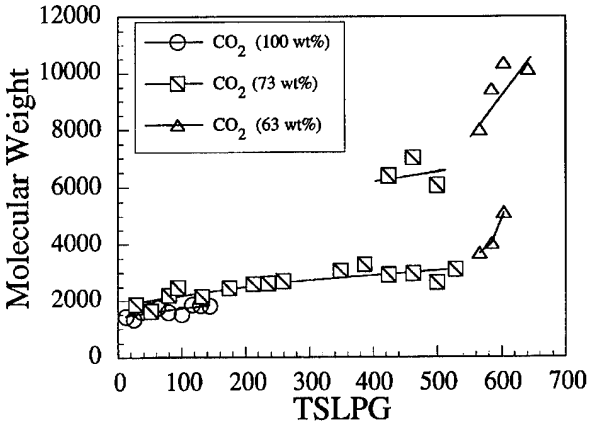

Figure 3. The molecular weight of L-PLA as a function of TSLPG (total standard liters solvent per gram polymer) using extraction conditions of 55 °C and 200 bar. Line is best fit through data.

sorbance at 340 nm correlates linearly with the L-lactic acid concentration from a standard calibration curve.

RESULTS AND DISCUSSION

Solubility of L-PLA in Supercritical Fluid Mixtures. The main goal of this solubility study was to determine the feasibility of dissolving L-PLA in CO_2/$CHClF_2$ solvent mixtures. The $CHClF_2$ content in the solvent mixture ranged from 10 to 40 wt %. The range of compositions, extraction temperature, and extraction pressure used in this work was always well within the binary solvent's one-phase region, as calculated with the Peng–Robinson equation of state.[33,34] In previous work, using the same experimental apparatus and commercial L-PLA ($\overline{M}_w$ = 5000), the concentrations of polymer in the supercritical solution were determined to be solubility values since no changes in the concentration were observed when the flow rate was increased two-fold.[2] Since the solute is a polymer, the role of polydispersity was first examined, and thus the solubility of L-PLA in CO_2/$CHClF_2$ mixtures was measured as a function of processing time and solvent composition. As already observed[2] with commercial L-PLA, preconditioning was necessary before the molecular weight of the extracted material and the solubility stabilized over the course of the experiments. Thus, in this section, we discuss the preconditioning of the polymer, and its solubility, as a function of process variables (pressure, temperature, and solvent composition).

The solubility and molecular weight of L-PLA at extraction conditions of 55 °C and 200 bar are shown in Figures 2 and 3 as a function of processing time. Three sets of measurements corresponding to different solvent compositions (CO_2–$CHClF_2$) are shown in these figures. The first set of measurements corresponded to preconditioning with pure CO_2. As the processing time (as measured by total standard liters solvent per gram polymer [TSLPG]) increased from 0 to 150, the molecular weight of the extracted polymer increased from 1300 to 1900, and the solubility decreased from 0.045 to 0.002 wt %. The addition of $CHClF_2$ (27 wt %) in the second set of measurements increased both the solubility and the extracted polymer's molecular weight. The solubility was typically 2–4 times that of the solubility when using pure CO_2. In this second set of measurements using CO_2 (73 wt %)–$CHClF_2$ (27 wt %), the initial solubility ranged from 0.01 to 0.02 wt % and decreased to less than 0.005 wt % after 500 TSLPG. The molecular weight of the extracted polymer increased from 1800 to 3100 as TSLPG increased from 0 to 500. At a TSLPG of 400, a second polymer fraction of higher molecular weight (6000–7000) first appeared in the supercritical solvent. As the quantity of extracted polymer with 2000–3000 molecular weight decreased and the presence of this polymer fraction became undetectable, only polymer of the higher molecular weight was extracted. The material remaining after preconditioning with CO_2 (73 wt %) - $CHClF_2$ (27 wt %) (second set of extractions) was used as starting material for a third set of experiments with CO_2 (63 wt %)–$CHClF_2$ (37 wt %). In this third set of measurements, the solubility was initially 0.015 wt % and decreased to 0.003 wt % after 100 additional TSLPG. Two molecular weight fractions were obtained ($\overline{M}_w$ = 3500 and 8000). The lower molecular weight fraction increased from 3500 to 5200 while the higher molecular weight fraction increased from 8000 to 10000 after <100 TSLPG of processing with the solvent mixture. After 150 TSLPG of processing with CO_2 (63 wt %)–$CHClF_2$ (37 wt %), only polymer of $\overline{M}_w \approx 10000$ was extracted.

All morphological studies with L-PLA in this work were done using material preconditioned so that the precipitated material had a molecular weight similar to that of the starting L-PLA polymer. Polydispersity, even though it was as low as 1.15, played a significant role in the amount of preconditioning necessary to achieve equiv-

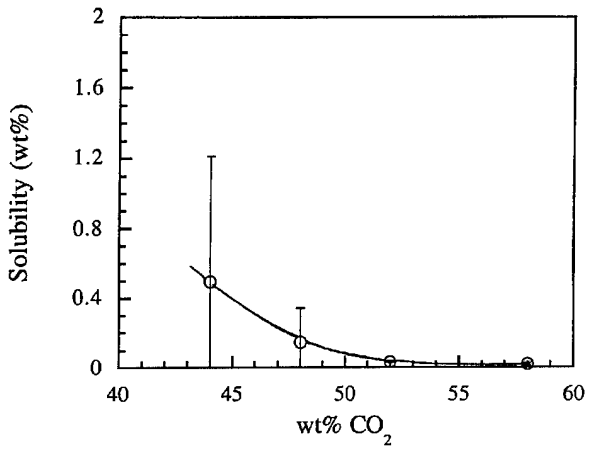

Figure 4. Solubility of L-PLA as a function of CO_2 solvent composition at 55 °C and 200 bar.

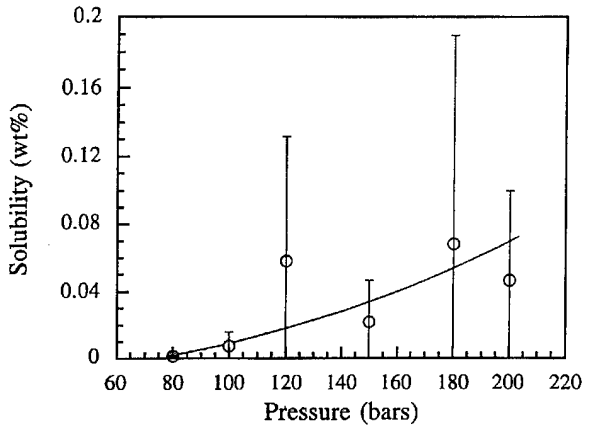

Figure 5. Solubility of L-PLA in 60 wt % CO_2–40 wt % $CHClF_2$ at 55 °C.

alency between the molecular weights of the extracted and starting materials. The amount of preconditioning necessary to extract L-PLA of $\overline{M}_w$ = 10000 was significant (~650 TSLPG CO_2-$CHClF_2$ flow). This is a reflection of the continuous mode of operation of the apparatus. Alternatively, in semi-batch operation, the dissolution of the solute in a liquid solvent, followed by heating and compression to supercritical conditions, and expansion,[1] could significantly minimize preconditioning. However, the low solubility would require either extremely large (batch) reservoirs or (in the case of L-PLA) flammable solvents with high critical temperatures (e.g., acetone).

Once the molecular weight of the extracted material reached that of the starting polymer, the effect of process conditions on solubility was examined. Both the effect of solvent composition at a fixed pressure and temperature, and of pressure and temperature at a fixed solvent composition, were measured. Figure 4 shows the measured solubility as a function of solvent composition at extraction conditions of 55 °C and 200 bars. As the $CHClF_2$ content increased, the solubility increased. Figures 5 and 6

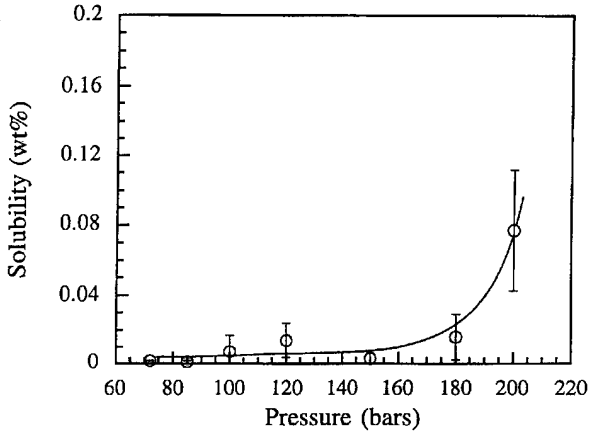

Figure 6. Solubility of L-PLA in 60 wt % CO_2–40 wt % $CHClF_2$ at 65 °C.

TABLE II
Solubility (wt %) of L-PLA in 60 wt % CO_2–40 wt % $CHClF_2$

Pressure (bar)	Solubility at 55 °C	Solubility at 65 °C
72		0.0018 (.0003)
80	0.0014 (.0006)	
85		0.001 (.00086)
100	0.0076 (.0008)	0.0072 (.0095)
120	0.0582 (.0733)	0.0137 (.0102)
150	0.0221 (.0246)	0.0031 (.0030)
180	0.0683 (.121)	0.0158 (.0135)
200	0.0467 (.053)	0.0770 (.0345)

* Numbers in parenthesis are standard deviations. Results are averages of 3–10 samples.

show the solubility in 60 wt % CO_2–40 wt % $CHClF_2$ as a function of pressure at 55 and 65 °C, respectively. The overall solubility was lower at 65 °C than at 55 °C, indicating retrograde behavior. Table II summarizes the solubility data at these two temperatures. General solubility trends were determined using CO_2–$CHClF_2$ solvent mixtures, but the error associated with measurements where the solubility was greater than 0.02 wt % tended to be quite significant.

The main source of error in the solubility experiments using CO_2-$CHClF_2$ was the difficulty in maintaining constant flow rates of two fluids into the same apparatus. During collection of solubility data, the flow exited at the crystallizer bypass (a micrometering valve) which occasionally became partially plugged with precipitate, decreasing the flow rate and increasing the pressure. The back pressure regulator controlling the CO_2 flow compensated for the increased pressure by decreasing the CO_2 flow, resulting in a sudden increase in the $CHClF_2$ concentration of the solvent. This was prevented by visually monitoring the flow and adjusting the micrometering

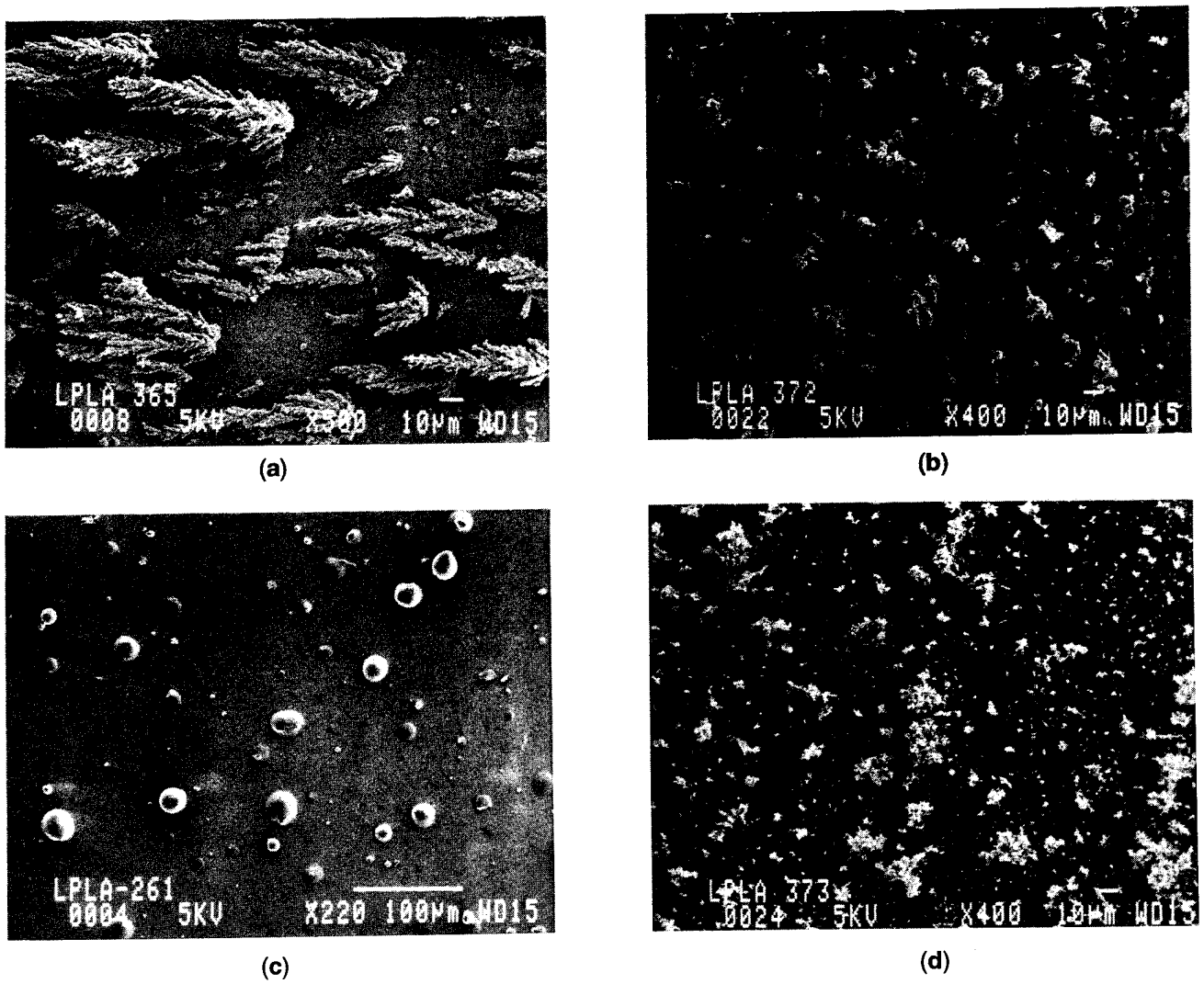

Figure 7. L-PLA dendrites (**a**), microparticles (**b**), microspheres (**c**), and agglomerates (**d**) produced by RESS using orifices as the expansion device.

valve to offset any partial plugging. Since visual monitoring was not perfect, small drops in flow rates were occasionally observed, resulting in variations in the CO_2-$CHClF_2$ composition. These variations had a large effect on solubility. The largest errors in the solubility measurements occurred at conditions of high solubility (55 °C, high pressures, and high $CHClF_2$ concentrations).

MORPHOLOGY OF RESS PROCESSED L-PLA

The unprocessed polymer (L-PLA, $\overline{M}_w \approx 10000$, $\overline{M}_w/\overline{M}_n = 1.15$) consisted of microparticles of less than 10 µm in size. The morphology of RESS-processed L-PLA was examined as a function of the following process variables: dimensions of the expansion device, preexpansion temperature, and solvent composition. The extraction pressure ranged from 165 to 240 bar, the extraction temperature was 55 °C, and the preexpansion temperature ranged from 80 to 140 °C. In all of these experiments, the supercritical solution was expanded to nearly atmospheric pressures (<5 bar). Previous work has shown that, for typical extraction pressures (e.g., >150 bar), particle morphology is quite insensitive to variations in post-expansion pressures when this variable is reduced below 50 bar.[15,35] The results of orifice experiments are presented first, followed by experiments using capillaries. In all of these experiments, the material in the column was preconditioned until the extracted polymer's molecular weight was similar to that of the starting material.

The orifices had a length-to-diameter ratio (*L/D*) of 9.4 based on a nominal diameter of 27 µm and a length of 0.254 mm. All of these experiments were conducted using an extraction temperature of 55 °C. At all extraction pressures (165–240 bar), three types of morphology were observed: microparticles, microspheres, and dendrites. Here, we define microparticles as nonspherical objects of polyhedral shape. Within each pressure range, the effects of preexpansion temperature and CO_2 content in the solvent mixture were examined.

The formation of dendrites occurred only under two sets of conditions: either at the high extraction pressure range (230–240 bar) or at low CO_2 content (<75 wt %). Both sets of conditions correspond to higher polymer solubility. If dendrites were formed by growth and coagulation of primary particles, then higher solubilities would indeed be expected to lead to enhanced coagulation because the quantity of precipitate would be greater. The formation of dendrites was found to be independent of: 1) the crystallizer temperature, which ranged from 20 to 60 °C at the different conditions; and 2) the preexpansion temperature, which ranged from 85 to 145 °C. The crystallizer and preexpansion temperatures are related. Higher preexpansion temperatures resulted in the fluid having higher temperatures after exiting the orifice, and thus higher temperatures in the crystallizer. The glass-transition temperature, T_g, of the L-PLA material used in this study is 65 °C[34] (see also Table VII). The bulk crystallizer temperature never exceeded this value. Thus, any eventual softening of the polymer and fusing of individual particles can only have occurred in the immediate vicinity of the exit of the expansion device's exit. Figure 7a shows an example of typical dendrites. The size of the dendrites indicated that they formed outside the orifice since the overall dimensions were larger than the orifice's diameter.

Microspheres and microparticles were formed over a range of conditions: at all the pressures examined, at preexpansion temperatures of 100 and 120 °C, and at crystallizer temperatures of 25 and 40 °C. Microspheres and microparticles were observed when using a CO_2 content higher than 75 wt %. Examples of microsphere and microparticle formation are shown in Figures 7b and 7c. The microparticles of Figure 7b, obtained from extraction pressures of 170–175 bars, preexpansion temperature of 98 °C, crystallizer temperature of 25 °C, and a 78 wt % CO_2 solvent mixture, ranged from 2 to 10 μm. Figure 7c shows examples of microspheres of 10–30 μm in diameter. In the background, microparticles smaller than 1 μm can be seen. This precipitate was obtained at extraction pressures of 205–210 bars, a preexpansion temperature of 114 °C, and a solvent composition of 90 wt % CO_2. The larger microparticles and microspheres (10–30 μm) appeared as individual particles, not as growth or agglomerations of submicron particles. Agglomerates, which appeared as clusters of micro-particles without the branching of dendrites, were observed only at extraction pressures of 190–200 bars. Figure 7d shows agglomerates of fine particles obtained by using 94 °C as preexpansion temperature, 17–21 °C as crystallizer temperature, and a CO_2 content of 68 wt %. In this experiment, the size of the primary particles appeared to be submicron while the clusters were 10–20 μm.

To summarize the observations using orifices, the rapid expansion of supercritical CO_2–$CHClF_2$ solutions of L-PLA using orifices of *L/D* ratio ≈ 9.4 resulted in a range of morphologies, including microparticles, microspheres, agglomerates, and dendrites. Dendrites were formed at process conditions favoring high polymer solubility, over a wide range of preexpansion and crystallizer temperatures. Control over particle morphology was found to be extremely difficult in orifice experiments. In some samples exhibiting dendrite formation, small microparticles and microspheres were found as well, and in samples of microparticles and microspheres, a range of particle size was observed. Dendrites were formed in the expansion jet after exiting the orifice since the dimensions of dendrites were larger than the orifice. Thus, it is important to understand the free-jet expansion after leaving the orifice in order to relate process conditions to particle morphology. Significant challenges in controlling morphology arise because precipitation occurs after the orifice, where the fluid undergoes an isentropic free-jet expansion and then mixes with background gas.[1,27,36] As the expansion jet decelerates to subsonic velocities, a series of shock waves occur. It is estimated that a significant fraction of the fluid's density drop occurs in that region.[1] Small changes in conditions (initial temperature, pressure, solubility) could affect the profiles in this region, and thus, the morphology of the precipitate. This will be discussed further in the next section when comparisons between experiments and model results are made.

Capillaries are of interest in RESS because the dimensions of the expansion device control the expansion process, and these dimensions can be varied to examine their effect on particle formation. The higher *L/D* ratio of capillaries with respect to orifices leads to a larger density drop within the expansion device, and hence to particle formation under more controllable conditions. The morphology of L-PLA precipitated from capillary tubing was explored under a range of process conditions, including the *L/D* ratio of the tubing. Capillary tubing with inner diameters of 30 and 50 μm was used. In these experiments, the extraction pressure was varied from 175 to 220 bars, the extraction temperature was maintained at 55 °C, the concentration of CO_2 in the CO_2–$CHClF_2$ solvent mixture was varied from 40 to 80 wt %, the preexpansion temperature was varied from 85 to 145 °C, and the crystallizer temperature ranged from 10 to 50 °C. A key observation in all the experiments with capillaries was that dendrites were rarely formed. In the few cases where they were formed, the dendrites' dimensions were much smaller than those produced with orifices. The results of experiments using 30-μm i.d. capillaries are presented first, followed by the results of experiments with 50-μm capillaries.

Table III summarizes experiments using the 30-μm capillaries. The length of the capillary tubing was varied between 5 and 15 mm, resulting in *L/D* ratios between 167 and 500. All experiments with the 30-μm capillary were performed at the same extraction pressure (190–210 bar) and temperature (55 °C). The precipitate's morphology at these conditions consisted of either microspheres or

TABLE III
Summary of L-PLA Experiments Using 30-μm Diameter Capillary

CO_2 (wt %)	*P* (bars) extract	L (mm)	*L/D*	*T* (°C) preexp.	*T* (°C) cryst.	Particles
81	190–200	15	500	126	43–45	μpart: 2–5 μm
82	190–195	15	500	130	39–41	μpart: 2–5 μm
76	190–200	15	500	116	35–39	agglomerates 10–20 μm; μpart: 2–4 μm
76	190–195	15	500	115	33–38	μparticles 2–5 μm
76	190–200	15	500	100	19–24	agglomerates 10 μm; μpart: 1–4 μm
42	200–220	15	500	123	36–41	fibers
42	200	15	500	100	20–25	fibers
56	200	10.5	350	130	39–42	μparticles <10 μm
55	200–210	10.5	350	121	25–35	μparticles <10 μm
56	190–200	10.5	350	106	35–38	μsphere:10–100 μm; μpart < 1 μm
55	200	10.5	350	95–99	24–28	μspheres < 50 μm; μpart < 2 μm
56	190–200	10.5	350	85	25–31	μspheres: 10 μm; μpart < 1 μm
68	200	8	267	107	24–27	μspheres: < 30μm
61	200–210	8	267	95	22–30	μspheres < 10 μm
61	210	8	267	84	25–26	μspheres < 30 μm
54	200–210	7.5	250	120	30–35	μspheres < 100 μm; μpart
59	200–210	7.5	250	98	20–27	μspheres < 50 μm
62	210–220	7.5	250	87	29–30	μspheres < 50 μm
59	200–210	7.5	250	85	24–28	μspheres < 100 μm
62	200–210	7.5	250	84	20–27	μparticles < 10 μm
69	200–210	6	200	100	29–30	μspheres < 100 μm
65	195–210	5	167	114	19–25	μspheres < 30 μm
70	195–210	5	167	93	12–17	μspheres < 50 μm
70	190–210	5	167	94	22–25	μspheres < 50 μm; μpart< 1 μm

microparticles, but some examples of agglomerates were obtained as well. At the highest *L/D* ratio, 500, either microparticles or agglomerates of microparticles were obtained with solvent content greater than 75 wt % CO_2. The preexpansion temperature, which was varied from 100 to 126 °C, had no noticeable effect on the morphology. Figure 8a shows examples of microparticles, and of agglomerates of microparticles. The microparticles and primary particles of the agglomerates were all less than 10 μm.

Decreasing the length of the 30-μm capillary to 10.5 mm or *L/D* of 350 led to precipitation of either microspheres or microparticles. Microparticles were obtained at high preexpansion temperatures (120–130 °C) and microspheres were formed at the lower preexpansion temperatures (85–105 °C). Figures 8b and 8c show examples of microspheres and microparticles formed using this *L/D* ratio. The microspheres of diameters 10–50 μm had a smooth outer surface against a backdrop of smaller microparticles (1–2 μm). The microparticles (10–20 μm) had irregular shapes with smaller microparticles in the background (1–2 μm). At a capillary *L/D* ratio of 350, there was a progression from microparticles to microspheres as the preexpansion temperature was decreased. At lower lengths (8 to 5 mm) of the 30 μm capillary (or *L/D* ratios between 267 and 167), the precipitate was dominated by formation of microspheres. The microspheres were obtained at a range of preexpansion temperatures (85–120 °C). The microspheres showed some variations in size and morphology. Some samples consisted of microspheres smaller than 30 μm in diameter. Other samples consisted of microspheres with a wider distribution of particle sizes (10–100 μm) (Figure 8d). The larger microspheres were clearly formed outside the capillary since their diameters are greater than that of the expansion device. In addition, a small amount of microparticles was usually observed in these samples.

In summary, using the 30-μm capillary, a range of morphologies was produced by RESS. At high *L/D* ratios (i.e., 500), only microparticles and agglomerates of microparticles were obtained, regardless of the preexpansion temperature. At an *L/D* ratio of 350, microparticles were formed at high preexpansion temperatures and microspheres were formed at low preexpansion tempera-

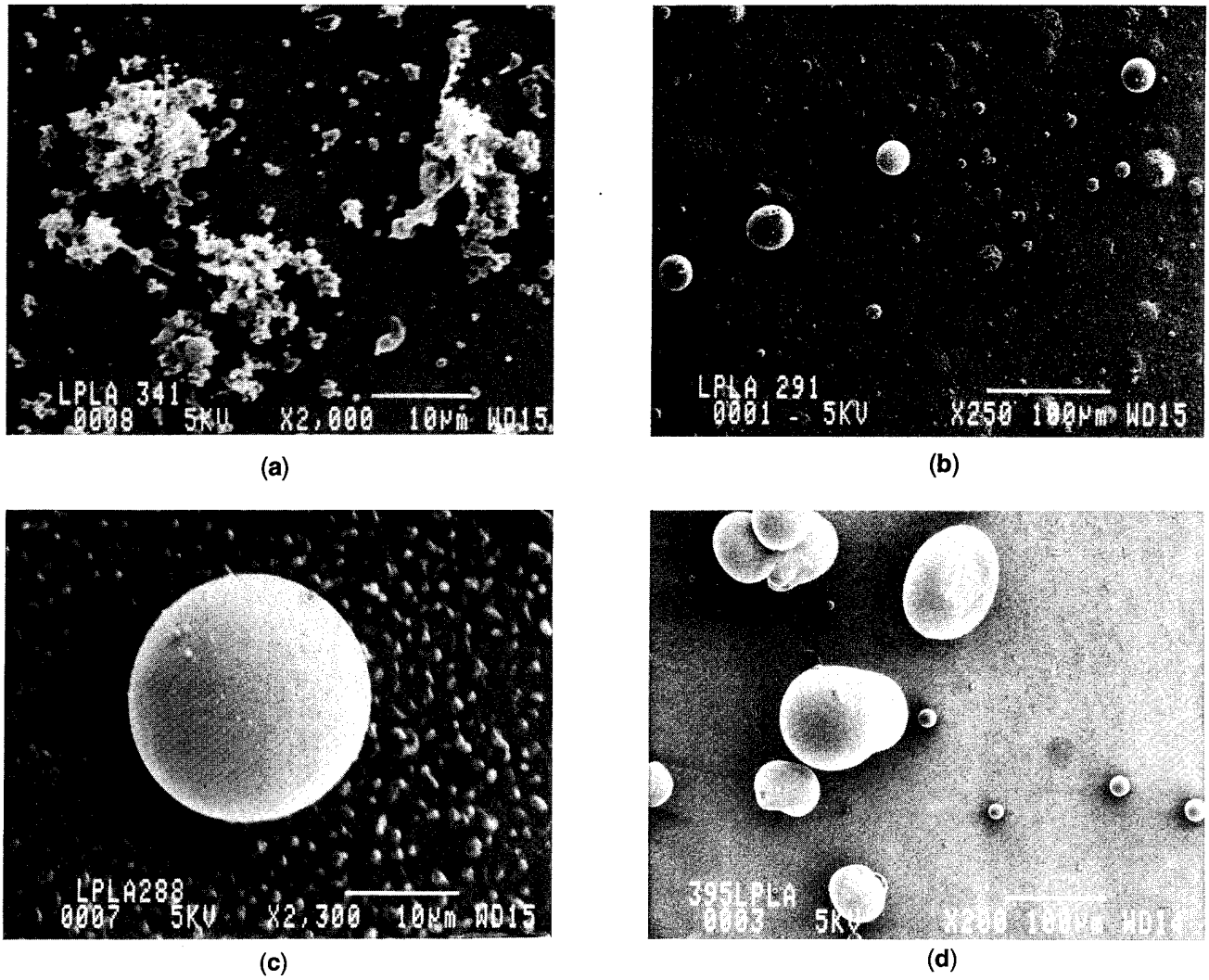

Figure 8. L-PLA microparticles (**a**) and microspheres (**b–d**) produced by RESS using capillaries as the expansion device.

tures. This transition occurred at 110–120 °C. At low *L/D* ratios (<300), microspheres were the dominant morphology. Variations in the shape and surface characteristics in the microparticles and microspheres were observed. Based solely on the size of the microspheres, precipitation at high *L/D* ratios could have occurred within the capillary, and precipitation at low *L/D* ratios most likely took place outside the capillary. The relative amount of precipitation which occurred within and outside the capillary could not be quantified. The appearance of several morphologies within a single experiment suggests that precipitation occurred in both regions.

Experiments with the 50-µm capillary showed similar trends. Tables IV and V summarize the conditions and results of the experiments using this capillary diameter. Lengths from 6 to 15 mm were examined (or *L/D* ratios from 300 to 120). Using capillaries with *L/D* ratio of 300, microparticles were produced at all the preexpansion temperatures examined (93–145 °C), and with solvent mixtures containing 50–80 wt % CO_2. Some small dendrites (<30 µm) were produced in a few experiments. Since the overall dimensions of these dendrites were found to be smaller than the capillary diameter, it is possible that they formed within the capillary, unlike the dendrites formed using orifices. There was evidence of a few microspheres (<10 µm) among the microparticles. Microparticles dominated the morphology at this *L/D* ratio using the 50-µm capillary, while both microparticles and microspheres were produced at this *L/D* ratio with a 30 µm capillary. Changing the preexpansion temperature did not cause any transition in morphology with the 50 µm capillary. Microspheres dominated the morphology at *L/D* ratios below 300. The conditions of these experiments were preexpansion temperatures of 100–120 °C, and solvent mixtures containing 60–85 wt % CO_2. The microspheres ranged in diameter from <10 µm to ≈100 µm.

An analysis of variance (ANOVA)[37] was performed to determine if any of the process variables could be correlated with either the size or the morphology of the precipitated powder. Three sets of data were examined: 1) the microsphere and microparticle data from the experiments

TABLE IV
Summary of L-PLA Experiments using 50-μm Diameter Capillary with *L/D* = 300

CO_2 (wt %)	*P* (bars) extract	*L* (mm)	*L/D*	*T* (°C) preexp.	*T* (°C) cryst.	Particles
78	195–205	15	300	132	42–47	μparticles: 10–30 μm
69	200	15	300	145	48–52	μparticles
67	200	15	300	140	45–50	μpart: < 5 μm
64	200	15	300	107	25–30	μpart: < 2 μm
70	200	15	300	114	33–34	μpart: < 50 μm; small dendrites
76	200	15	300	122	40–44	μpart; < 10 μm, agglomerates
82	170–200	15	300	93	24–30	μpart: < 20 μm
61	200	15	300	101	25–30	μpart: < 5μm, some dendrites, few μspheres: 10 μm
62	210	15	300	105	19–25	μpart: < 5 μm, some dendrites
72	200	15	300	100	22–24	μpart: < 10 μm
69	200	15	300	100	25–27	μpart: < 10 μm
71	200	15	300	112	28–34	μpart: < 10 μm
66	200–220	15	300	125	34–38	μpart: < 10 μm; few μspheres
66	200–220	15	300	125	34–38	μpart: < 10 μm; few μspheres
58	220	15	300	100	30–35	μpart: < 10 μm
58	210–220	15	300	110	34–36	μpart: < 10 μm
53	200–220	15	300	120	35–40	μpart: < 10 μm
52	200–220	15	300	106	34–38	μpart: < 10 μm

TABLE V
Summary of L-PLA Experiments Using 50-μm Diameter Capillary with *L/D* < 300

CO_2 (wt %)	*P* (bars) extract	*L* (mm)	*L/D*	*T* (°C) preexp.	*T* (°C) cryst.	Particles
85	170–190	10	200	114	35–40	μspheres: < 10 μm
70	200–215	10	200	101	21–24	μspheres: < 10 μm
70	180–200	10	200	97–100	29–31	μpart: < 10 μm, some agglomerates
63	190–200	10	200	115	37–41	μspheres; μpart: < 10 μm
68	200–210	10	200	115	35–40	μpart: 10 μm
70	200–210	8.5	170	105	25–30	μspheres: < 100 μm
65	150–170	8	160	113	37–48	μpart: < 20 μm; μspheres: < 30 μm
61	180–200	8	160	113	20–29	μspheres: < 20 μm, some μpart
74	200	7	140	117	25–31	μspheres: < 100 μm
69	190–200	6.5	130	122	33–44	μspheres: < 30 μm, few μpart
59	200–210	6	120	115	25–30	μspheres: < 100 μm

with the 30-μm capillaries (Table III), 2) the microsphere data from the experiments with the 50 μm capillaries (*L/D* ≤ 200; Table V), and 3) all data from the experiments using both 3- and 50-μm capillaries (Tables III–V). For each experiment, the particle size was taken to be that of the largest individual particle. ANOVA (95% confidence limit) showed no correlation of precipitate particle size with preexpansion temperature, crystallizer temperature, or solvent composition. A correlation between the *L/D* ratio and the precipitate particle size was found. As the *L/D* ratio decreased, there was an increase in the size of the particles in the precipitate. A similar analysis was done using the precipitate morphology as the dependent variable. This analysis was done by assigning morphology results as "1" for microparticles and "2" for microspheres. A correlation (95% confidence limit) was found between morphology and *L/D* ratio. A correlation between morphology and preexpansion temperature was not considered statistically significant in this analysis. However, ANOVA of the two variables (preexpansion temperature and *L/D* ratio) taken jointly did show a correlation with particle morphology. These statistical correlations will be explained in the next section in terms of the fluid dynamics of the solvent's expansion.

Using capillary tubing, a set of conditions was identified (low *L/D* ratio and low preexpansion temperature) which favored precipitation of microspheres, and another set of conditions (high *L/D* ratio and high preexpansion

TABLE VI
Summary of Morphology as a Function of *L/D* Ratio and Preexpansion Temperature*

30 μm	*L/D* = 500	*L/D* = 350	*L/D* = 267	*L/D* = 250	*L/D* = 167
130 °C	*P*	*P*			
120 °C	*P*	*P*		*S*	*S*
110 °C	*P*	*S*	*S*		*S*
100 °C	*P*	*S*	*S*	*S*	
90 °C		*S*	*S*	*S*	*S*
50 μm	***L/D* =300**	***L/D* = 200**	***L/D* =170**	***L/D* =140**	***L/D* = 120**
140 °C	*P*				
130 °C	*P*				
120 °C	*P*			*S*	
110 °C	*P*	*S*			*S*
100 °C	*P*	*S*	*S*		
90 °C	*P*				

* *P* = μparticles; *S* = μspheres

TABLE VII
Properties of L-PLA after RESS Processing

L-PLA	$\overline{M}_w$	T_m (°C)	T_g (°C)	$\overline{M}_w/\overline{M}_n$
starting material	10200	162.5	62	1.15
precipitate	10800	164.2	68	1.14
material left in column	10000	166.3	62	1.13

temperature) which led to formation of microparticles, as summarized in Table VI. The size of microspheres or microparticles provides some information on the precipitation mechanism. If the precipitate's dimensions were greater than the inner diameter of the capillary, it is reasonable to assume that a significant amount of precipitation must have occurred after exiting the capillary. On the other hand, if the particles were smaller than the inner diameter of the capillary, it is possible, but not certain, that the particles were formed within the capillary. The fluid dynamical model in the next section sheds light on this important question.

The properties of the original and processed L-PLA polymer were characterized by NMR, DSC, surface area, and hydrolysis experiments. The NMR showed the peaks of precipitated and starting L-PLA to be identical. The methyl hydrogens and the backbone hydrogen were found at 1.58 and 5.16 ppm. RESS processing of preconditioned L-PLA with CO_2-$CHClF_2$ solvent mixtures did not significantly change the molecular weight and polydispersity of the polymer, as shown in Table VII. The precipitate was examined after extraction with 600 total standard liters CO_2 and 140 total standard liters $CHClF_2$ per gram L-PLA, and the remaining material in the column was examined after extraction with 530 total standard liters CO_2 and 72 total standard liters $CHClF_2$ per gram L-PLA. The time and solvent composition used in preconditioning prior to the collection of the precipitate for these characterization tests were typical of the morphological studies with L-PLA.

The hydrolysis rate (rate of degradation of L-PLA) of the starting and precipitated L-PLA were also measured. The starting material and the precipitated L-PLA showed a dramatically lower rate of degradation than the commercial polymer studied earlier.[2] Figure 9 shows the degradation rate as a function of time. The starting material was only 9% degraded after 4000 h. Two different samples of L-PLA precipitated using capillaries degraded at an even slower rate: less than 1% after 3500 h. The overall low degradation rates were a result of the polymer's low polydispersity. Material with a wider distribution of molecular weights will degrade faster because of the faster hydrolysis of the low molecular weight components. While synthetic L-PLA of $\overline{M}_w$ = 10000 provided uniformity in molecular weight and polydispersity between the starting material and the experimental samples, the hydrolysis rate suggests that it may only be suitable for controlled drug-release of very long time periods.

Other properties of the precipitate which are related to the degradation rate are the surface area and the degree of crystallinity. The surface area of precipitated L-PLA was slightly higher than that of the starting material. The values for two precipitate samples were 8.8 and 7.6 m^2

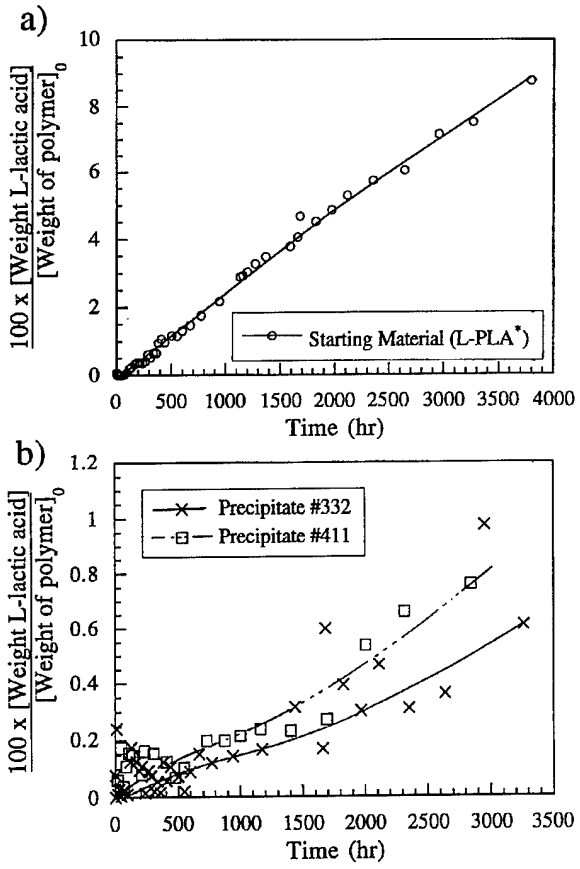

Figure 9. Hydrolysis rate for (**a**) L-PLA and (**b**) precipitated L-PLA. The *y*-axis gives 100 times the weight of L-lactic acid in solution divided by the weight of L-PLA initially in solution.

g^{-1}, respectively, while the starting material had a surface area of 7.3 m^2 g^{-1}. Thus, it was unlikely that surface area played a role in the lower hydrolysis rate. The relative crystallinity in the starting and precipitated L-PLA was determined by calculating the net area in the DSC peaks (net difference between the area of endothermic peaks and exothermic peaks).[38] The starting material had a lower heat capacity than the precipitate (6.3 vs. 11.4 mcal K^{-1} mg^{-1}), indicating that the precipitate was more crystalline. Wide angle x-ray diffraction showed little difference between the relative crystallinity in the starting and precipitated L-PLA because of the high noise-to-signal ratio. The increased crystallinity of the precipitate may have contributed to the lower degradation rate while the precipitate's increased surface area did not result in higher degradation rates.

Characterization of the precipitate indicated that most of the physical properties that we investigated (molecular weight, polydispersity, T_m, T_g) were comparable to that of the starting polymer (see Table VII). However, the hydrolysis rate of the precipitate was considerably lower than that of the starting material, which may result from the increased crystallinity of the processed polymer.

MODEL

The fluid dynamics of the expansion process is basic to a full understanding of RESS. The evolution of temperature, pressure, and density along the expansion device provides information on the approximate location of precipitation, as well as on the solvent's state of aggregation during particle formation. To explain the experimental observations, we model the solvent flow as a steady, adiabatic, one-dimensional expansion. The calculations yield velocity, temperature, pressure, and density profiles along the expansion device. Particle nucleation and growth are not incorporated into this model. Thus, predictions about the solid phase are qualitative. A full model incorporating nucleation and growth, which allows the calculation of particle-size distributions, has recently been proposed.[28] In this section we first describe the fluid mechanical model, and then show how it can be used to interpret some experimental observations.

The expansion device (orifice or capillary) is a constant-area duct, and changes in fluid properties are brought about by wall friction.[39] The flow is modeled as a one-dimensional adiabatic expansion. In RESS, a supercritical fluid flows through a capillary at velocities of order 100 m s^{-1}, leading to residence times within the capillary of 10^{-5}–10^{-4} s. In contrast, the characteristic time for heat transfer is typically on the order of a second.[34,40] Thus, adiabatic conditions prevail to an excellent approximation, resulting in negligible heat interactions.[41] Our approach is based on the recent fundamental study of polymer RESS by Lele and Shine,[11] who used a similar model for the solvent expansion. The dynamics of expansion from a large-diameter reservoir into and through a constant-area duct with friction are described by mass, momentum, and energy balances

$$U\frac{d\rho}{dx}+\rho\frac{dU}{dx}=0 \tag{1}$$

$$\rho U\frac{dU}{dx}+\frac{dP}{dx}=\frac{-2fU^2\rho}{d} \tag{2}$$

$$\frac{\rho U}{M}\frac{dh}{dx}-U\frac{dP}{dx}=\frac{2fU^3\rho}{d} \tag{3}$$

where ρ is the mass density, U is the velocity, x is the distance along the capillary, P is the pressure, d is the diameter of the orifice or capillary, f is the Fanning friction factor, M is the molecular weight of the fluid, and h is the molar enthalpy. The fluid's nonideality is conveniently described by the Peng–Robinson equation of state (PR EOS)[33]

$$P=\frac{RT}{v-b}-\frac{a}{v^2+2vb-b^2} \tag{4}$$

where v is the molar volume (= M/ρ), R is the gas constant, and a, b are parameters of the PR EOS. The constants, a and b, are defined as follows

$$b = 0.0778\frac{RT_c}{P_c} \tag{5}$$

$$a = a(T_c)\alpha(T_r,\omega) \tag{6}$$

$$a(T_c) = 0.45724\frac{R^2T_c^{\,2}}{P_c} \tag{7}$$

$$\alpha(T_r,\omega) = \left[1+m\left(1-T_r^{0.5}\right)\right]^2 \tag{8}$$

where T_r is the reduced temperature (T/T_c) and m = 0.37464 + 1.54226ω − 0.26992ω^2, with ω, the acentric factor.[42] Using departure functions[43] and the PR EOS, the enthalpy is expressed in terms of density and temperature. Upon differentiation of eq 4, eqs 1–4 constitute four first-order ordinary differential equations which can be solved for the spatial derivatives of four unknowns (dP/dx, dT/dx, $d\rho/dx$, dU/dx). Equation 4 is used in its (T, P, ρ) explicit form. Solving this linear system with a given set of initial conditions (T_1, P_1, U_1, ρ_1) yields four coupled ordinary differential equations,

$$\frac{d\mathbf{Y}}{dx} = F\{\mathbf{Y}\} \tag{9}$$

where $\mathbf{Y} = \{P, T, U, \rho\}$. A fourth-order Runge Kutta method[44] is used to advance the calculation along the axis of the expansion device.

In order to start the calculation, the conditions at the entrance of the expansion device must be known. Since the diameter of the tubing before entering the expansion device (~0.2 cm) is much greater than that of the expansion device itself (0.003–0.005 cm), the velocity in the tubing (~1 cm s^{-1}) is negligible in comparison to the velocity in the capillary (~10000 cm s^{-1}), the fluid in the tubing is essentially stagnant and the tubing can be considered a reservoir. Thus, the reservoir conditions are the extraction pressure and the preexpansion temperature (or P_0 and T_0). The PR EOS yields the reservoir's molar volume (v_0) from P_0 and T_0. Enthalpy and entropy balances yield the conditions at the entrance (T_1, v_1). The losses between the reservoir and the capillary entrance are thus calculated assuming isentropic flow. Therefore, we have

$$s(T_0,v_0) = s(T_1,v_1) \tag{10}$$

$$h(T_0,v_0) = h(T_1,v_1) + 1/2U_1^{\,2}M \tag{11}$$

where s and h are the molar entropy and enthalpy. The entropy and enthalpy are calculated using departure functions. The velocity, and thus, the kinetic energy, at the entrance is calculated from the input flow rate since the diameter at the entrance is known. The entropy and enthalpy balances are then non-linear equations in two unknowns (T_1, v_1). The Newton–Raphson method is used to obtain T_1 and v_1.

For subsonic flow in a constant-area duct, the fluid will accelerate due to friction. The maximum velocity the fluid can attain is sonic velocity at the exit of the capillary. Sonic velocity occurs when the fluid's velocity equals the speed of sound. The speed of sound, c, is given by

$$c^2 = \left(\frac{\partial P}{\partial \rho}\right)_S . \tag{12}$$

A useful quantity for the calculations is the Mach number, defined as the ratio of the fluid's velocity to the speed of sound. At sonic conditions, the Mach number is unity. At this point, the maximum flow rate is achieved and process conditions such as downstream pressure do not change the flow rate. This condition is known as choked flow. The governing equations can be written in terms of the Mach number and a singularity occurs when Mach number reaches unity. This corresponds to the physical impossibility of accelerating the fluid from subsonic to supersonic conditions in a constant area duct.[41]

Since all the experiments reported here involved expansion to atmospheric pressure and choked flow, the algorithm for these calculations is to input the reservoir conditions (extraction pressure and preexpansion temperature), the expansion device's diameter and length, and then iterate the value for the flow rate until the Mach number at the exit equals one.[11]

Since the experiments used a mixture of two solvents (CO_2 and $CHClF_2$), the solvent is described in this model as a single fluid with an effective critical temperature (T_c), critical pressure (P_c), acentric factor (ω), and heat capacity (c_p).[43,45,46] The liquid–vapor phase envelopes for CO_2–CHF_2Cl were calculated with the Peng–Robinson equation for mixtures to provide a consistency check for the calculated conditions at the exit of the expansion device. In order to calculate vapor–liquid equilibrium, experimental CO_2–$CHClF_2$ data, available for a limited range of pressures (10–70 bar) and temperatures (273–333 K),[47] were fitted to obtain the binary interaction coefficient, k_{ij} = 0.02, for the Peng–Robinson EOS. The mixture's (>60 wt % CO_2) true critical temperatures and pressures are within 3 and 1% of the effective values.

The reliability of the model was checked by measuring the exit temperature with a thermocouple (Type J, Omega Engineering). The thermocouple was placed not

TABLE VIII
Comparison Between Calculated and Measured Exit Temperatures

Solvent	Reservoir Pressure (bar)	Pre-expansion T (K)	Exit T (K) Calculated	Exit T (K) Measured	% Error
CO_2	180	359.1	256.8	281.1	9.5
CO_2	190	376.1	273.3	289.1	5.8
CO_2	198	399.1	296.8	300.4	1.2
CO_2	200	415.1	316.7	301.6	4.8
85 wt % CO_2	188	358.1	260.3	255.3	1.9
85 wt % CO_2	188	376.1	273.1	283.6	3.8
85 wt % CO_2	193	394.1	291.9	292.2	0.1
85 wt % CO_2	195	415.1	316.5	306.0	3.3

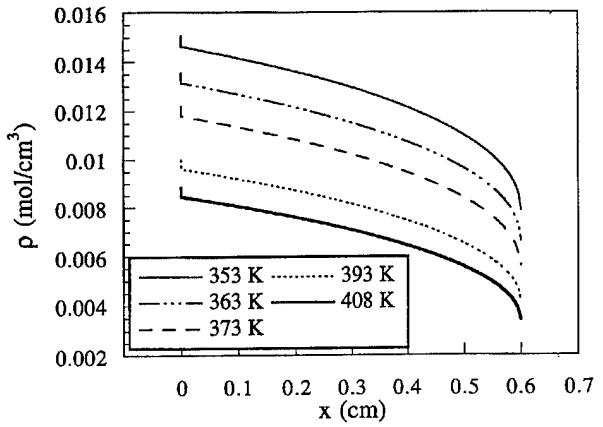

Figure 10. Calculated solvent density along the expansion device's axis (L/D = 200) as a function of preexpansion temperature at extraction pressure of 200 bar and solvent composition of 70 wt % CO_2.

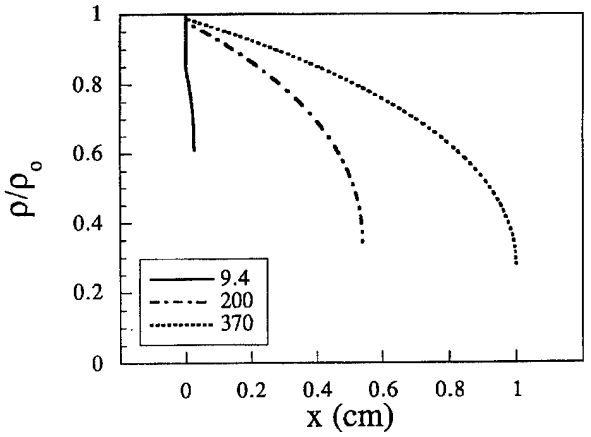

Figure 11. Calculated solvent reduced density profile along the expansion device's axis for orifices (L/D = 9.4) and capillaries (L/D = 200, 370) at preexpansion temperature of 120 °C, extraction pressure of 200 bar, and solvent composition of 70 wt % CO_2.

more than 2 mm away from the capillary exit. The fluid's measured exit temperature at different preexpansion temperatures and L/D ratios was compared to the calculated temperature. The best fit of calculated temperatures to the measured temperatures was obtained using a friction factor of 0.005. This value of the friction factor is identical to the one used by Lele and Shine,[11] who obtained excellent agreement between measured and calculated flow rates. Table VIII shows this comparison using a 50 μm × 20 mm (L/D = 400) capillary with pure CO_2, and with a 85 wt % CO_2–15 wt % $CHClF_2$ mixture. The error is within 10% and most measurements fall within 5% of the calculated temperature.

The independent variables in the calculations are the expansion device's length and diameter (and the resulting L/D ratio), the reservoir conditions, and the solvent's composition. Changing reservoir conditions affects the resulting density profile and pressure–temperature trajectory of the fluid as it travels along the expansion device. Increasing the preexpansion temperature shifts the density profile along the expansion device to lower densities. The fluid's density at the exit of the expansion device is lower as the reservoir temperature increases (Figure 10). As the preexpansion temperature increases, the net change in the pressure and temperature within the capillary decreases.

The RESS experiments with L-PLA were aimed at studying the effect of the L/D ratio, capillary diameter, and preexpansion temperature on product morphology (see Tables III–VI). The use of capillaries resulted in clear trends (e.g., high L/D ratio and high preexpansion temperature favored formation of microparticles) while trends were difficult to discern when using orifices. This observation is (at least partially) consistent with calculations based on the simple flow model presented here. The model predicts that conditions at the end of orifices are quite different from those that occur in capillaries. In Figure 11, we compare the density change along the expansion device starting from reservoir conditions of 220 bar and 110 °C for a typical orifice with L/D ratio of 9.4

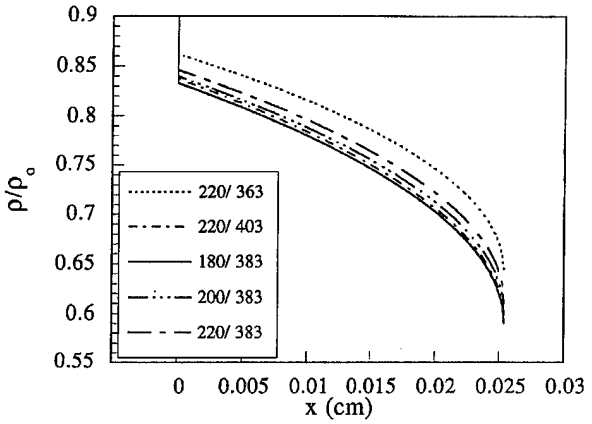

Figure 12. Calculated solvent reduced density profile along the orifice's axis (L/D = 9.4) as a function of extraction pressure (bar) and preexpansion temperature (K) at solvent composition of 70 wt % CO_2.

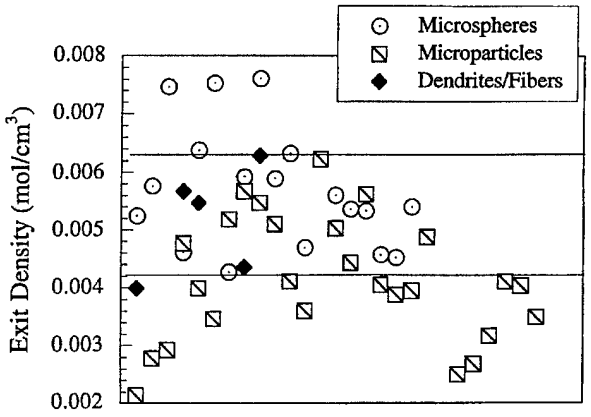

Figure 13. Calculated solvent exit density for all capillary experiments.

and D = 27 μm, with the corresponding quantity, but for capillaries with L/D ratios of 200 and 370. At the exit of the expansion device, ρ/ρ_0 (the density normalized to the density at the entrance of the expansion device) is 0.61 in the case of orifices and 0.31 in the case of a capillary with L/D ratio = 200. Thus, considerable expansion occurs after exiting the orifices. In contrast, considerable expansion occurs within capillaries with large L/D ratios. While the calculations behind Figure 11 are for specific reservoir conditions, this same trend (considerable expansion within capillaries and outside orifices) is observed at other reservoir conditions and can be considered typical in RESS.

In the case of orifices, there is a free-jet expansion to ambient conditions after the orifice.[10,27,36] The free-jet expansion consists of compression shock waves, and subsequent mixing with a lower pressure environment. The effect of process conditions on the expansion in the orifice is shown in Figure 12. The changes in the density profile are small. The changes in reservoir conditions do not appreciably affect the expansion path within orifices. Therefore, the variations in particle morphology using orifices are not reflections of the expansion within the orifices, but of the process conditions during the free-jet expansion. Since the fluid has appreciable density after exiting the orifice, solutes may still be dissolved, leading to precipitation in the free-jet expansion. Thus, uncontrolled morphologies such as dendrites, which are produced only with orifices, are likely to be the result of precipitation in an uncontrolled environment such as a free-jet expansion.

From Figure 11 it can be concluded that a significant density drop occurs within a capillary during RESS. Since the solvent power of a given fluid depends sensitively on its density,[17] the point where precipitation occurs can also be correlated with solvent density in the capillary. Thus, it is important to examine the effect of varying process conditions on the fluid's density profile within the capillary. The fluid's density within the capillary is affected by the key process variables (extraction pressure, preexpansion temperature, L/D ratio, and solvent composition), and is a convenient measurement of the aggregate effect of all these variables. The density at the end of the capillary was calculated for each of the experiments in Tables III–V. The exit densities are shown in Figure 13. The range of exit densities can be divided into three distinct regions. At low exit densities (<0.0042 mol cm^{-3}), only particles are formed. At high exit densities (>0.0063 mol cm^{-3}), only microspheres are formed. As will be shown, this lower exit density value corresponds closely to the solubility detection limit. At an intermediate exit density range (0.0042 mol cm^{-3} < ρ_{exit} < 0.0063 mol cm^{-3}), both microspheres and microparticles are produced. Other morphologies such as dendrites and fibers, also appear in this intermediate range. Microsphere formation involves appreciably more solvent expansion in the free jet outside the capillary than formation of microparticles. A statistical analysis of variance of exit density as an independent variable and morphology as a dependent variable showed a correlation which was significant with 95% confidence. Extending the analysis to the relationship between exit density and the size of the particles in the precipitate, a correlation was found between these two variables with 90% confidence.

The solubility data provide information on the supersaturation ratio and the point of precipitation. The solubility of L-PLA is plotted in Figure 14 as a function of solvent density (see Figures 5 and 6). While the error bars are large, the trend is clear. The solvent density is calculated using the Peng–Robinson equation. At a density of 0.004 mol cm^{-3} (threshold exit density below which only microparticles were formed), corresponding to data from measurements at extraction conditions of 65 °C and 72–85 bar, the solubility is very low (0.001–0.002 wt %). Since the solubility at this point is not that far from the detection limit (0.0005 wt %), it is likely that a significant amount of precipitation will have occurred. Above a density of 0.0063 mol cm^{-3} (corresponding to the threshold exit density above which only microspheres

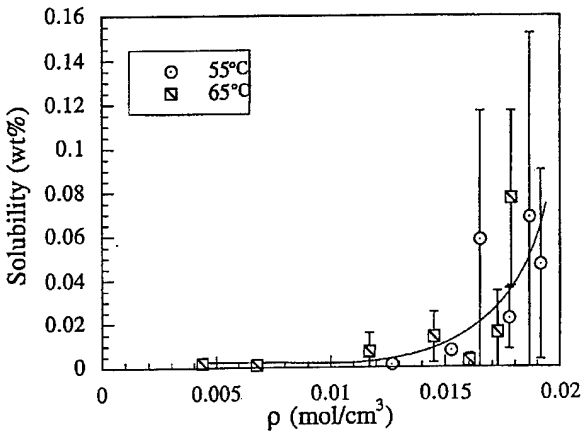

Figure 14. Solubility of L-PLA in 6 wt % CO_2–40 wt % $CHClF_2$ at extraction temperature of 55 °C and 65 °C, as a function of solvent density.

were produced), the measured solubility is not inconsistent with the hypothesis that material is still dissolved (and easily measurable), and that some precipitation must still occur upon further expansion. Thus, microspheres can be formed outside the capillaries while microparticles can be formed within the capillaries. Further evidence for formation of microspheres outside the capillaries can be found in the sizes of some of the microspheres (greater than the capillary's diameter). In contrast, the sizes of microparticles are smaller than the capillary diameter. The appearance of some microparticles with microspheres indicates that precipitation may occur within and outside the capillary. This is supported by an intermediate region of exit densities in which both microspheres and microparticles were found to be dominant.

COPRECIPITATION OF L-PLA AND PYRENE

The ultimate goal in the present research is to use the RESS technique as a route to polymeric microspheres or microparticles loaded with pharmaceuticals for controlled drug delivery applications. This idea is mentioned in a patent by Fischer and Müller.[48] Numerous studies have explored the RESS precipitation of pharmaceutical compounds.[14–16] Here, we have examined the RESS precipitation of L-PLA. Thus, the coprecipitation of polymers and pharmaceutical compounds to produce composite particles useful for drug delivery is a natural extension of this work. In our previous work using RESS coprecipitation to produce such devices, the effectiveness and uniformity of the distribution of drug particles in the polymer matrix was difficult to detect and control.[3] In the experiments to be described, pyrene was used as the nonpolymeric low-molecular-weight solute and L-PLA was used as the polymeric solute. The choice of pyrene as model solute is based on the fact that this substance is fluorescent. This, as will be explained below, allowed us to observe and assess the effectiveness and uniformity of pyrene's distribution in the polymer matrix as a function of process conditions, Thus, even though pyrene is of no biomedical interest, these experiments allow, for the first time, to investigate the relation between the distribution of an encapsulated solute in a matrix during RESS coprecipitation, and process conditions.

In the previous section, the process conditions which led to the formation of L-PLA microspheres and microparticles were explored. Conditions which led to a high exit density (i.e., low *L/D* ratio, low preexpansion temperatures) favored the formation of microspheres. Typical conditions leading to formation of L-PLA microspheres were extraction pressure of 200 bar, preexpansion temperature of 100 °C, and $L/D < 300$. Pyrene particles obtained at these conditions were small, on the order of 1–2 μm. Thus, the combination of L-PLA microspheres of up to 100 μm and pyrene microparticles of a few microns provided the correct size ratio of polymer to non-polymeric solute of interest in typical controlled drug-delivery devices. Since the maximum solubility of pyrene in CO_2 (≤0.3 wt %)[32] is of the same order of magnitude as that of L-PLA in CO_2–$CHClF_2$ mixtures (<0.1 wt %), the concentration in the exit fluid stream from the extraction column containing pyrene was diluted with CO_2 from a bypass line (see Figure 1). The level of dilution was controlled by setting the flow of CO_2 saturated with pyrene via a metering valve. A lower valve setting resulted in a high dilution ratio and a lower pyrene concentration in the mixture. The pyrene concentration in CO_2 as a function of valve setting at 65 °C and 200 bar ranged from <0.001 to 0.005 wt %. This was determined by independent calibration.[34] The solubility of pyrene in CO_2 at these conditions is 0.2 wt %.[32] In these experiments, therefore, the pyrene concentration was diluted by two orders of magnitude with respect to saturation.

Fluorescence microscopy was used to identify pyrene-rich regions within microspheres and microparticles. Figure 15 shows examples of such images with unprocessed L-PLA and pyrene. The image on the right is the transmitted light image; particles which block light appear as a dark object against a white background. The image on the left is the fluorescence image; particles which fluoresce appear white against a dark background. Since L-PLA is non-fluorescent and pyrene is fluorescent, the distribution of pyrene particles can be detected within the polymer precipitate by comparing transmission and fluorescent images of the same sample.

The column containing L-PLA was preconditioned (~600 TSLPG) until the extracted material had similar molecular weight as the starting material in the column. The extraction condition used was 200–210 bar, and 55 °C for column 1 and 65 °C for column 2. Column 1, containing L-PLA, was extracted with a CO_2–$CHClF_2$ mixture (60 wt % CO_2) and column 2, containing the pyrene, was extracted with CO_2. The effect of the pyrene concentration was examined by adjusting the setting of the col-

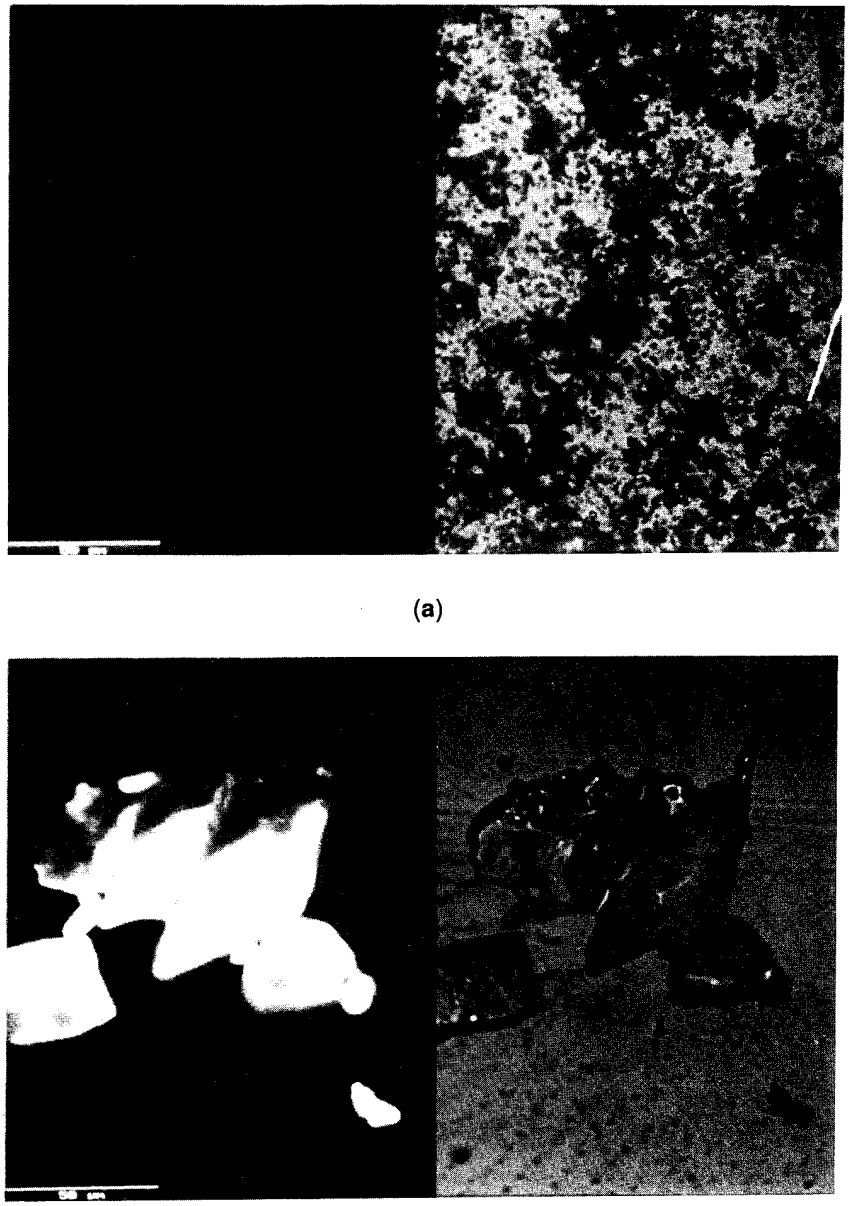

Figure 15. Fluorescence (left) and transmission (right) images of unprocessed **(a)** L-PLA and **(b)** pyrene.

umn 2 exit valve in this set of experiments. The preexpansion temperature was 107–110 °C, and the crystallizer temperature ranged from 24 to 30 °C. The diameter of the capillary was 50 μm and the *L/D* ratio was 200. After L-PLA particle formation began, the pyrene–CO_2 stream was added to the L-PLA solution stream and the combined mixture was preheated and expanded.

At low pyrene concentration (0.0008 wt % in CO_2), microspheres of L-PLA showed little or no fluorescence (Figure 16a). As the pyrene concentration was increased (0.0013 wt % in CO_2), the quantity of fluorescence increased (Figure 16b). Some of the fluorescence originated from the polyhedral-shaped pyrene particles and some from polymeric microspheres (pyrene does not precipitate as microspheres). Thus, fluorescent microspheres contained pyrene within an L-PLA matrix. At pyrene concentration of 0.0017 wt %, the quantity of fluorescence (as measured by total area of fluorescence) was similar to that found in samples obtained at a lower pyrene concentration (0.0013 wt %). Further increases in the pyrene concentration in CO_2 to 0.0021 wt % resulted in an increase in both the intensity (brightness) and quantity of fluorescence. Figure 16 (c,d) shows examples of such polymer microspheres. Microspheres from these samples examined by SEM showed smooth surfaces, occasionally in contact with a few submicron particles.[34] Thus, the uniform florescence observed cannot be attributed to pyrene particles on the surface of the microspheres.

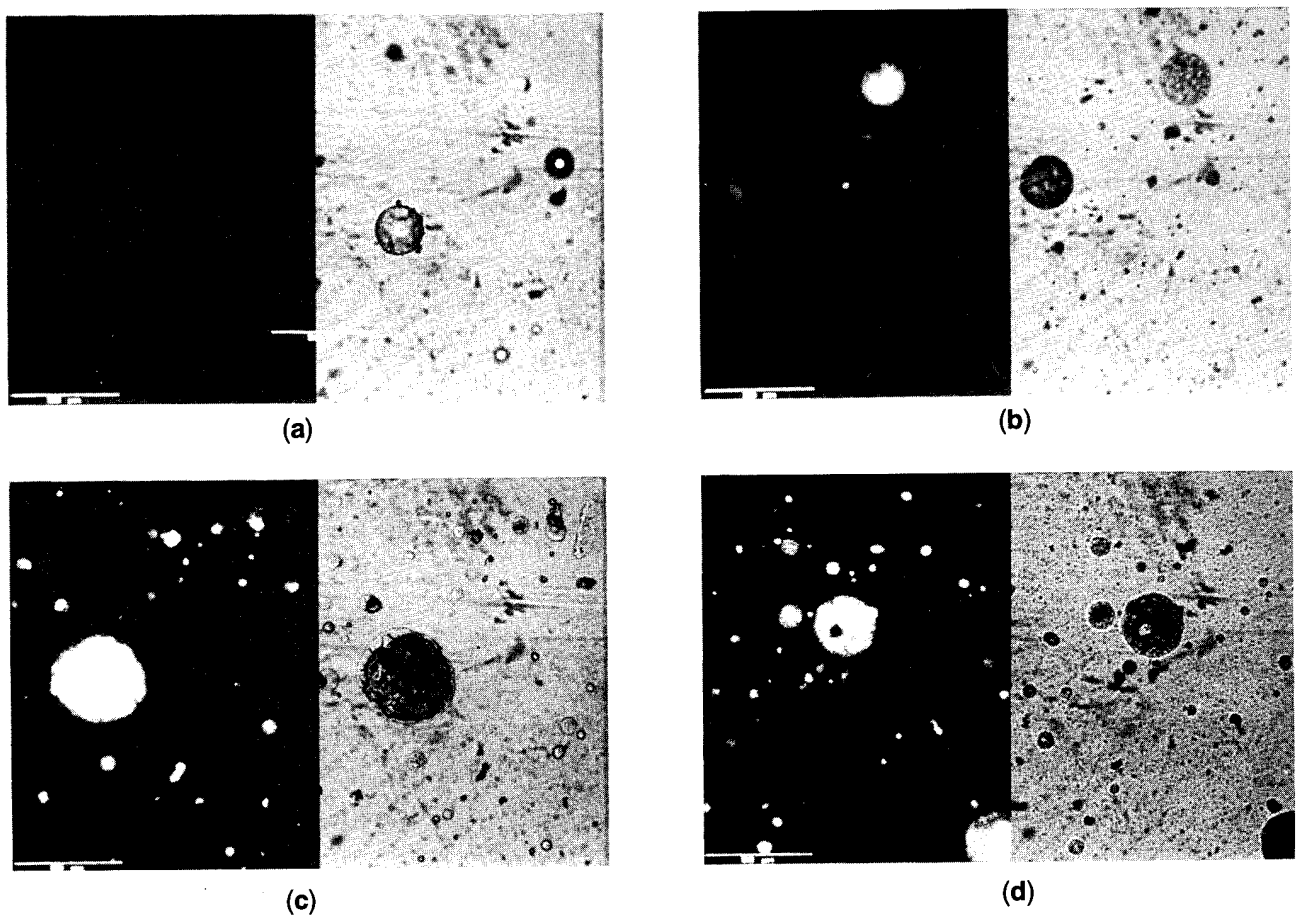

Figure 16. Fluorescence and transmission images of L-PLA -pyrene microspheres precipitated at pyrene concentrations in CO_2, **(a)** <0.001 wt %, **(b)** ≈0.0013 wt %, and **(c, d)** >0.002 wt %. The L-PLA was extracted with 60 wt % CO_2–40 wt % $CHClF_2$ at 200–210 bar and 55 °C, and pyrene was extracted with CO_2 at 200–210 bar and 65 °C and diluted to above concentrations. A preexpansion temperature of 107–110 °C and a capillary of *L/D* = 50 μm) were used.

Thus, in coprecipitation experiments leading to the formation of polymeric microspheres, microspheres with and without fluorescence were observed. The former were more readily observed at high pyrene concentration, and the latter at low pyrene concentration. The result that increasing pyrene concentration led to increases in the fluorescence of microspheres is intuitively obvious. As the pyrene concentration in CO_2 increased above 0.002 wt %, pyrene agglomerates separate from the microspheres were also observed. This suggests that there is a limit to the amount of pyrene that can be incorporated into a microsphere. These observations point to the need for a better understanding of coprecipitation in RESS. A minimum requirement is knowledge of the solubility of both compounds in the supercritical carrier, hence of their respective supersaturation profiles during a given expansion. Such a calculation, even while it ignores the possibility of heterogeneous nucleation of one component triggered by earlier homogeneous nucleation of the other one, would at least provide a starting point for the estimation of overall precipitate compositions.

The results of this coprecipitation study confirm[48] the feasibility of RESS processing for producing composite particles consisting of a polymeric matrix and embedded non-polymeric solutes. The L-PLA microspheres clearly showed the uniform incorporation of pyrene within the matrix. Thus, we have shown that under process conditions leading to polymer microspheres (<100 μm) and small microparticles (<5 μm) of non-polymeric solute, complete and uniform incorporation of solutes within a polymer matrix is feasible by RESS coprecipitation. This is very important from the point of view of controlled drug release applications.

SUMMARY

The RESS processing of L-PLA, a biodegradable polymer of interest in controlled drug-delivery applications, has been explored in supercritical CO_2–$CHClF_2$ solutions. After sufficient preconditioning (ca. 800 total standard liters solvent per gram polymer), there was minimal change in the polymer's solubility (<0.1 wt %) and molecular weight in solution (ca. 10000), permitting an examination of the effects of process conditions on the morphology of precipitated L-PLA. We examined the influence of three key process variables (the *L/D* ratio of the expansion device, the preexpansion temperature, and the

solvent composition) on the morphology of the precipitated L-PLA. Precipitation using orifices (L/D = 9.4) resulted in a range of morphologies (microspheres, microparticles, dendrites, and agglomerates). Increasing the extraction pressure and $CHClF_2$ content in the solvent favored dendrite formation. The size of the RESS-processed polymer pointed to precipitation in the free jet expansion region after exiting the orifice. Dendrite formation rarely occurred using capillaries, and in the few cases where it did, the dendrites were smaller than those formed using orifices. Using a 30 μm diameter capillary tube, microparticles were obtained at an L/D ratio of 500 at all preexpansion temperatures examined. Decreasing the L/D ratio of the 30-μm capillaries to 350 led to precipitation of microspheres only at preexpansion temperatures below 110 °C. At L/D ratios below 300 using 30-μm capillaries, microspheres dominated the precipitation at all preexpansion temperatures. Increasing the diameter of the capillaries to 50 μm resulted in similar trends as with the 30-μm capillaries. At high L/D ratios (300), only microparticles were formed regardless of the preexpansion temperature. At lower L/D ratios (<300), microsphere formation dominated at all the preexpansion temperatures examined. These trends can be rationalized by examining the solvent's properties during the expansion within the capillary or orifice.

The influence of the same process variables was explored using a simple model of solvent expansion in the capillary incorporating the dynamics and thermodynamics of compressible flow. The transition between microparticles and microspheres was found to be correlated with the fluid's density at the exit of the capillary. At low densities (<0.004 mol cm^{-3}), only microparticles were formed, and at higher exit densities (>0.0063 mol cm^{-3}), only microspheres were formed. Formation of microspheres thus appears to involve a considerable amount of free-jet expansion.

In experiments with L-PLA and pyrene, fluorescence and transmission microscopy allowed the observation of pyrene in the coprecipitate. In coprecipitation experiments, the different morphologies of the polymer and pyrene precipitate showed clearly the uniform incorporation of pyrene microparticles within polymer microspheres. This work is the first comprehensive study of the effects of process conditions on the composite powders formed by RESS coprecipitation. These results are a starting point towards a more complete understanding of the mechanism of coprecipitation using RESS. More importantly, the results of these coprecipitation experiments point to the feasibility of the main application of coprecipitation by RESS, that is the formation of intimate mixtures and composite particles of multiple components.

ACKNOWLEDGMENTS

PGD gratefully acknowledges the support of the National Science Foundation (Grant # CTS-9000614) and the Air force Office of Scientific Research (Grant AASERT F49620-93-1-0454). JWT gratefully acknowledeges the support of the National Science Foundation for a graduate fellowship.

REFERENCES

(1) Matson, D. W.; Fulton, J. L.; Petersen, R. C.; Smith, R. D. *Ind. Eng. Chem. Res.* **1987**, *26*, 2298.
(2) Tom, J. W.; Debenedetti, P. G. *Biotechnol. Prog.* **1991**, *7*, 403.
(3) Tom, J. W.; Lim, G.; Debenedetti, P. G.; Prud'homme, R. K. In *Supercritical Fluid Engineering Science*; Kiran, E.; Brennecke, J. F., Eds.; ACS Symposium Series 514; American Chemical Society: Washington DC, 1992.
(4) Matson, D. W.; Petersen, R. C.; Smith, R. D. *Adv. Cer. Mater.* **1986**, *1*, 242.
(5) Matson, D. W.; Petersen, R. C.; Smith, R. D. *Mater. Lett.* **1986**, *4*, 429.
(6) Matson, D. W.; Petersen, R. C.; Smith, R. D. *Adv. Ceram.* **1987**, *21*, 109.
(7) Petersen, R. C.; Matson, D. W.; Smith, R. D. *J. Am. Chem. Soc.* **1986**, *108*, 2100.
(8) Adschira, T.; Kanazawa, K.; Arai, K. *J. Am. Ceram. Soc.* **1992**, *75*, 1019.
(9) Adschira, T.; Kanazawa, K.; Arai, K. *J. Am. Ceram. Soc.* **1992**, *75*, 2615.
(10) Brand, J. I.; Miller, D. R. *Thin Solid Films* **1988**, *166*, 139.
(11) Lele, A. K.; Shine, A. D. *AIChE. J.* **1992**, *38*, 742.
(12) Petersen, R. C.; Matson, D. W.; Smith, R. D. *Polym. Eng. Sci.* **1987**, *27*, 1693.
(13) Krukonis, V. Paper 140f. AIChE Meeting, San Francisco, November, 1984.
(14) Larson, K. A.; King, M. L. *Biotechnol. Prog.* **1986**, *2*, 73.
(15) Mohamed, R. S.; Halverson, D. S.; Debenedetti, P. G.; Prud'homme, R. K. In *Supercritical Fluid Science and Technology*; Johnston, K. P.; Penninger, J. M. L., Eds.; ACS Symposium. Series 406; American Chemical Society: Washington, DC, 1989.
(16) Chang, C. J.; Randolph, A. D. *AIChE J.* **1989**, *35*, 1876.
(17) Kumar, S. K.; Johnston, K. P. *J. Supercrit. Fluids* **1988**, *1*, 15.
(18) Harvey, A. H. *J. Phys. Chem.* **1990**, *94*, 8403.
(19) Debenedetti, P. G. *AIChE J.* **1990**, *36*, 1289.
(20) Langer, R. *Science* **1990**, *249*, 1473.
(21) Rosen, H. B.; Kohn, J.; Leong, K.; Langer, R. In *Controlled Release Systems: Fabrication Technology*, Vol. II; Hsieh, D., Ed.; CRC: Boca Raton, FL, 1988.
(22) Larger, R. S.; Wise, D. I. *Medical Applications of Controlled Release*, Vol. I, Classes of Systems; CRC: Boca Raton, FL, 1984.
(23) Langer, R.; Peppas, N. *Rev. Macromol. Chem. Phys.* **1983**, *C23*, 61.
(24) Juni, K.; Nakano, M. *CRC Crit. Rev. Ther. Drug Carr. Sys.* **1987**, *3*, 209.
(25) Arshady, R. *J. Controlled Release* **1991**, *17*, 1.

(26) Tom, J. W.; Debenedetti, P. G. *J. Aerosol Sci.* **1991**, *22*, 555.
(27) Murphy, H. R.; Miller, D. R. *J. Phys. Chem.* **1984**, *88*, 4474.
(28) Kwauk, X.; Debenedetti, P. G. *J. Aerosol Sci.* **1993**, *24*, 445.
(29) Dubois, Ph.; Jacobs, C.; Jerome, R; Teyssie, Ph. *Macromolecules* **1991**, *24*, 2266.
(30) Jacobs, C.; Dubois, Ph.; Jerome, R.; Teyssie, Ph. *Macromolecules* **1991**, *24*, 3027.
(31) Johnston, K. P.; Ziger, D. H.; Eckert, C.A. *Ind. Eng. Chem. Fundam.* **1982**, *21*, 191.
(32) Bartle, K. D.; Clifford, A. A.; Jafar, S. A. *J. Chem. Eng. Data* **1990**, *35*, 355.
(33) Peng, D.; Robinson, D. B. *Ind. Eng. Chem. Fundam.* **1976**, *15*, 59.
(34) Tom, J. W. Ph.D. Thesis, Princeton University, 1993.
(35) Halverson, D. H. M.S. Thesis, Princeton University, 1989.
(36) Randall, L. G. In *Chemical Engineering at Supercritical Fluid Conditions*; Paulaitis, M. E.; Penninger, J. M. L.; Gray, R. D., Davidson, P. Eds.; Ann Arbor Science: Ann Arbor, MI, 1983.
(37) Box, G. E. P.; Hunter, W. G.; Hunter, J. S. *Statistics for Experimenters*; John Wiley & Sons: New York, 1978.
(38) Sperling, L. *Introduction to Physical Polymer Science*; John Wiley & Sons: New York, 1986.
(39) Shapiro, A. H. *The Dynamics and Thermodynamics of Compressible Fluid Flow*, Vol. 1; Ronald Press Co.: New York, 1953.
(40) Holman, J. P. *Heat Transfer*; McGraw-Hill: New York, 1990.
(41) Saad, M. A. *Compressible Fluid Flow*; Prentice-Hall: Englewood Cliffs, NJ, 1985.
(42) Pitzer, K. S. *J. Am. Chem. Soc.* **1955**, *77*, 3427.
(43) Reid, R. C.; Prausnitz, J. M.; Poling, B. M. *The Properties of Gases and Liquids*; McGraw-Hill: New York, 1987.
(44) Press, W. H.; Flannery, B. P.; Teukolsky, S. A.; Vetterling, W. T. *Numerical Recipes*; Cambridge University: Cambridge, 1989.
(45) Li, C.C. *Can. J. Chem. Eng.* **1971**, *19*, 709.
(46) Kreglewski, A.; Kay, W. B. *J. Phys. Chem.* **1969**, *73*, 3359.
(47) Nohka, J.; Sarashina, E.; Arai, Y.; Saito, S. *J. Chem. Eng., Japan* **1973**, *6*, 10.
(48) Fischer, W.; Müller, B. W. U.S. Patent 5 043 280, 1991.